NASA CR-54132

Quarterly Progress Report No. 3

BEHAVIOR OF VARIOUS ADSORBATES ON METAL SUBSTRATES

by

C. J. Bennette
R. W. Strayer
L. W. Swanson

Prepared for

Lewis Research Center, NASA
Cleveland 35, Ohio

CONTRACT NAS3-5902

Field Emission Corporation

McMinnville, Oregon

Requests for copies of this report should be referred to

National Aeronautics and Space Administration
Office of Scientific and Technical Information
Attention: AFSS-A
Washington, D.C. 20546

NASA CR-54132

Quarterly Progress Report No. 3
For the Period
1 December 1964 to 28 February 1965

BEHAVIOR OF VARIOUS ADSORBATES ON METAL SUBSTRATES

by

C. J. Bennette
R. W. Strayer
L. W. Swanson

Prepared for

Lewis Research Center, NASA
Cleveland 35, Ohio

20 April 1965

CONTRACT NAS3-5902

FIELD EMISSION CORPORATION
Melrose Avenue at Linke Street
McMinnville, Oregon

TABLE OF CONTENTS

LIST OF ILLUSTRATIONS

LIST OF ILLUSTRATIONS (continued)

PURPOSE

The primary aims of this work are to investigate metallic adsorption and sputtering of several refractory metals and to relate this knowledge (as it applies) to the understanding of vacuum voltage breakdown and leakage currents between high voltage electrodes coated with various adsorbates. Thus, the work breaks down into four separate tasks which include: (1) vacuum breakdown studies; 2) studies of the surface kinetics of adsorbed layers by field emission techniques; 3) investigation of sputtering of metallic surfaces by a combination of field electron and ion microscopy and 4) studies of electron interactions with single and multi-component adsorbed layers on metallic surfaces.

ABSTRACT

24124

In attempting to relate the theory of field emission initiated vacuum voltage breakdown to the experimental results a calculation had to be made in order to determine the effect of the electron space charge at emission levels sufficiently high that an arc could occur. When the effect of space charge is considered, the experimental results are shown to agree in trend with theoretical predictions concerning anode vs cathode initiated breakdown. Preliminary work is also reported concerning the effect of varying the electrode material from copper to tungsten.

The work function variation with coverage for cesium on rhenium and molybdenum has been measured; the shape of the resulting curves are similar to the one for tungsten, but with a slight shift in minimum toward low coverages in the case of rhenium. In addition, an investigation of the adsorption and desorption of thin mercury films on molybdenum substrates has established that (1) mercury adsorbed on molybdenum raises the work function; (2) for coverages above a monolayer mercury is mobile at 77°K; (3) applied fields of 25 Mv/cm or greater cause growth of mercury protrusions from the mobile layer at 77°K for certain coverages; and (4) all mercury is completely desorbed from molybdenum at 650°K.

Field ion microscope investigations of xenon ion sputtering of tungsten have resolved sputtering detail as fine as individual atom displacements, and have determined amount of both surface and interior damage done as functions of ion energy and surface crystallographic direction. These studies indicate an optimum ion energy, for which most of the energy is transferred through the tungsten tip, causing damage on the side away from the bombardment beam.

Measurements of electron desorption cross sections for cesium on clean tungsten over a range of temperatures and coverages for 294 volt electrons show no effect. Cross sections for electron desorption of cesium on tungsten are less than 6×10^{-22} cm^2.

AUTHOR →

PROGRESS TO DATE

Vacuum Voltage Breakdown Studies

A theory of field emission initiated vacuum voltage breakdown has been formulated which predicts within certain limits the occurrence of a cathode or anode initiated arc between electrodes with varying degrees of surface roughness. The boundary between anode and cathode initiated breakdown is affected only by the value of the field enhancement factor of localized emitting protrusions. Since preliminary experimental results from a fixed gap spacing copper electrode tube seemed to confirm the general features of the theory, a more detailed study ensued in which significant theoretical parameters could be varied in a controlled manner. The latter study in which both clean and cesium covered molybdenum electrodes were used indicated that although experimental results followed theoretically predicted trends, it was necessary to include the effect of electron space charge in order to obtain reasonable numerical agreement between experiment and theory.

Early in the contract the field emission nature of the pre-breakdown gap currents between clean and cesium-covered molybdenum electrodes was established for currents from 1.0×10^{-10} to 1.0×10^{-3} amps under the following conditions: gap spacings from 1.6 to 19.6 mils, cesium coverages corresponding to work functions from 4.20 (clean Mo) to 1.4 ev, varying degrees of surface roughness related to field enhancement factors from 10 to 155, and both polarities of electric field. The effect of electric field on the equilibrium coverage reported previously[1] has been observed in pre-breakdown current measurements, and is most pronounced at low coverages for which cesium migrates away from the high field region at the protrusion tip at temperatures above 250°K.

This investigation was extended to include a study of pre-breakdown current between copper electrodes in a fixed gap spacing diode with a gap spacing of 4.5 mils in which the field emission nature of the gap current was established. It was found that enhancement factors as low as 10 are possible on copper electrode surfaces, depending upon their prior treatment.

In order to study the effect of the electrode material on the nature of the pre-breakdown as well as the arc phenomena, a variable gap spacing tube was built in which one electrode was made of copper while the other was made of tungsten. Preliminary measurements taken in an ambient helium pressure indicated that under conditions such that an anode initiated arc would be expected, the current density of the cathode at breakdown, which can be related to the temperature of the anode, was significantly higher when the tungsten electrode was the anode than it was when the copper electrode was the anode. An interesting phenomenon was observed when the copper electrode had been damaged by an arc. Short range disorder resulting from an arc is healed at room temperature in copper by removing the electric field for a short

period of time, while a similar amount of damage is not healed when the copper electrode is cooled to $\sim 77^{\circ}K$. A similar effect was noticed previously[2] for tungsten at $800^{\circ}K$. It is interesting to note that the ratio of the temperatures at which this disorder can be healed is roughly the ratio of the respective melting temperatures of the two metals.

In extending the study from the stable pre-breakdown condition into the region of the actual arc, it was found that for d.c. voltages an anode power density was reached at which the current began to increase exponentially with time at a constant applied voltage. Thus far no completely satisfactory explanation for this phenomena can be made. However, it is a phenomena that is dependent solely upon the power density at the anode, since changing the cesium coverage from zero to more than one monolayer, allowing the anode or the cathode to contaminate, changing the temperature of either electrode, varying the gap spacing and/or the enhancement factor all have no noticeable effect. Since the I-V data is reproducible after the instability has occurred, the cathode is not altered. Calculated magnitudes of photon-electron effects are sufficiently small to preclude the possibility of a regenerative process due to this effect alone.

Studies of the Surface Kinetics of Adsorbed Layers

Activation energies of surface diffusion have been performed over a range of cesium coverages on tungsten by utilizing pulsed field emission current variations with time as a measure of the end point. The results confirmed earlier measurements[1] of a similar nature on molybdenum substrates, where it was found that the activation energy for surface diffusion was essentially independent of underlying cesium coverage; however, a variation in the pre-exponential of the rate equation was observed which accounts for the variation of the diffusion rates with coverage in the manner observed earlier.

The variation of work function change with cesium coverage on single crystallographic planes have been completed on the (110) and (100) planes of tungsten. These results have been compared with some of the existing theories, although some problems were encountered when attempting to establish the absolute coverage since the results suggest a difference in coverage between the two planes. This variation in coverage is such that the (110) plane has greater than average coverage whereas the (100) plane has less than average coverage. An empirical relationship between the maximum work function change and local substrate work function was formulated and appears to have validity for a variety of adsorbate-substrate systems.

The work function variation with coverage for cesium on rhenium and molybdenum has been measured; the shape of the resulting curves are

similar to the one for tungsten, but with a slight shift of the minimum toward lower coverages in the case of rhenium.

In an investigation of adsorption and desorption of thin mercury films on molybdenum substrates the work function changes, equilibration temperatures, and desorption temperatures have been measured as functions of relative mercury coverage, and activation energies have been obtained for diffusion and desorption at a low coverage. Some of the more interesting points established are: (1) mercury adsorbed on molybdenum raises the work function; (2) for coverages above a monolayer mercury is mobile at 77°K; (3) applied fields of 25 Mv/cm or greater cause growth of mercury protrusions from the mobile layer at 77°K for certain coverages; and (4) all mercury is completely desorbed from molybdenum at 650°K.

Sputtering Studies

An investigation of cesium ion sputtering of tungsten using field emission techniques has been initiated and has shown that surface roughness due to ion bombardment increases with ion energy for ion energies below 300 ev; extrapolation of the data indicates a threshold for ion roughening of the surface of about 20 ev. The slight damage done to the target surface by ion bombardment at energies below 1000 ev in these studies is removed by heating the target to relatively low temperatures, below 800°K. It has also been shown feasible to study sputtering of cesium-coated tungsten by field emission techniques.

Field ion microscope investigations of xenon ion sputtering of tungsten have resolved sputtering detail as fine as individual atom displacements, and have determined amount of both surface and interior damage done as functions of ion energy and surface crystallographic direction. These studies indicate an optimum ion energy, for which most of the energy is transferred through the tungsten tip, causing damage on the side away from the bombardment beam.

Electron Desorption Studies

A tube designed to study the interaction of low energy electrons with adsorbed layers of cesium and oxygen has been constructed and initial calibration measurements of the electron bombardment beam as a function of total accelerating voltage has been performed. The current density of the bombardment beam at the emitter varies between 7 and 30 ma/cm^2 as the accelerating voltage varies from 23 to 500 volts. This current density should be sufficient to detect electron-adsorbate reactions of moderately low cross section. Measurements of electron desorption cross sections

for cesium or clean tungsten over a range of temperatures and coverages for 294 volt electrons show no effect. Cross sections for electron desorption of cesium on tungsten are less than 6×10^{-22} cm^2.

VACUUM VOLTAGE BREAKDOWN STUDIES

In an earlier report[2] a theory was developed which predicted the circumstances under which the vacuum arc would be either cathode or anode initiated. It was shown that there existed a boundary value of surface field enhancement factor γ_o such that anode initiated breakdown would occur when $\gamma < \gamma_o$ and cathode initiated breakdown would occur when $\gamma > \gamma_o$. The maximum field enhancement factor γ_o was shown to depend significantly on the duration of the voltage pulse applied at the gap, particularly when the duration of the pulse was too short for the anode surface to reach steady state temperature. The shorter the pulse, the smaller the value of γ_o and the greater the probability of cathode rather than anode evaporation starting the arc process. Preliminary experimental work was described in which visual evidence of surface heating of copper electrodes was in agreement with theoretical predictions when the I-V data was analyzed and values of enhancement factor were determined. In more recent work an attempt has been made to establish experimentally the predicted relationship between the duration of the voltage pulse and the boundary value of the surface field enhancement factor γ_o. The results of these experiments are reported below.

EXPERIMENTAL PROCEDURES

The molybdenum electrode experimental tube has been described in the first quarterly report[3]. It is basically a diode consisting of a stationary 30 mil diameter spherical electrode and a moveable 200 mil diameter planar electrode, a cesium source, and a field emission microscope which can be used to monitor conditions within the tube. Both electrodes can be heated to remove surface contaminants and to smooth surface roughness. Microscopy observation of events taking place in the gap can be made by means of a flat window directly opposite the gap.

The I-V data was taken in low current ranges (from 10^{-10} to 10^{-6}) using only d.c. voltages but in the higher current range up to the actual arc the voltage was applied in single pulses of 2 to 10 μsec duration. There were two reasons for this: (1) if d.c. voltages were applied in the higher current regions, it was found that for anode power densities exceeding $\sim 3.0 \times 10^4$ watts/cm^2 the current increased exponentially with time at a constant voltage, therefore, by keeping the voltage pulse length short, current instability of this nature could be avoided and the I-V characteristics could be measured up to the values at which a destructive arc occurred, and (2) by varying either the amount of surface roughness

or the length of the pulse, the theoretically predicted relationship between enhancement factor and pulse length, which would determine whether an arc were anode or cathode initiated, could be investigated experimentally.

From the low current I-V data the work function ϕ, the surface enhancement factor γ, and an effective emitting area were determined using previously described methods[1]. The radius of the tip of an emitting protrusion is proportional to the square root of the emitting area, the factor of proportionality ranging from 1 - 4 for fields of from 30 - 100 Mv/cm. Knowing the field and the effective emitting area, a value can be calculated for the radius of an emitting protrusion. Using the relationship presented in the last quarterly[2] between the radius of the emitting protrusion and the radius of the anode spot, an anode current density can be calculated and thus an anode power density can be assigned for each value of I-V. The steady state temperature of the anode spot can then be determined from the relationship

$$\Delta T = \frac{W_a R_a}{K} \qquad (1)$$

where K is the thermal conductivity of the anode material, W_a is anode power density, and R_a is the radius of the anode spot. Since temperature is an important parameter in the theory of field emission initiated voltage breakdown, an independent method was needed to determine the accuracy of the calculations. A very rough check was made experimentally. The diameter of the anode spot was determined by measuring the diameter of the spot from which transition radiation[4] was observed using a telemicroscope with a micrometer eyepiece. After the spot size had been determined in this way, a polaroid filter was placed over the microscope objective positioned so that the plane-polarized transition radiation could not be transmitted to the eye. The onset of thermal radiation could thus be detected at some particular value of current and voltage. Although the small spot size and the low intensity of the radiation made it impossible to use any of the pyrometers available in this laboratory, a rough estimate could be made of the temperature from the color of the thermal radiation. This could be compared with the temperature calculated from equation (1). The size of the anode spot measured in this way agreed within 30% with that calculated from the relationship between cathode radius and anode radius, the measured radius being slightly larger. Thermal radiation became visible when the anode power density was such that ΔT was calculated to be 1250°C, that is, the temperature of the anode spot would be 1275°C. The radiation was bright yellow viewed through the optical system so that an estimate of the spot temperature on the basis of its color would correspond closely to that calculated.

In order to determine the effect of the properties of the electrode

material on the arc characteristics, the tube shown in Figure 1 was built in which one electrode was copper and the other was tungsten. The tube envelope was proportioned so that a transverse magnetic field could be applied across the gap to deflect the electron beam and control the power density at the anode. Preliminary d.c. measurements were made using this tube, however a leak developed in the bellows assembly and the tube had to be disassembled for repairs. Some data was obtained which will be reported below although the vacuum within the tube was only $\sim 10^{-8}$ torr.

RESULTS AND DISCUSSION

Clean and Cesium Covered Molybdenum Electrodes

When the voltage across the gap was increased continuously (d.c. case) it was found that as the anode power density reached some critical value, the current would increase exponentially with time at a constant voltage until the anode became sufficiently hot that an arc occurred. In order to establish that this "runaway" condition corresponded to a critical power density at the anode rather than to a critical current density, the work function of the surface was changed so that the voltage required to maintain a constant current was changed by a factor of five. The results showed that the power density required to initiate the "runaway" condition was constant and between 30 and 40 kw/cm^2 in magnitude.

The power density is related directly to the temperature of the bombarded surface as given in equation (1) so that one explanation for the onset of current instability might be that gas atoms on the anode surface are being thermally desorbed or ionized. If this were true, the desorbed atoms could either be ionized in the gap and sputter the emitting protrusion, or contaminate the protrusion and change its work function. Either event would be easily detected as a change in the slope of the Fowler-Nordheim plots before and after the onset of the current instability. However, the reproducibility of the I-V data showed that irreversible alterations of the cathode surface could not cause the increase in current. Further evidence for this is the fact that the critical anode power density remained constant and independent of the state of cleanliness of the anode surface.

In order to explain the increase in current with time only mechanisms which do not disturb the emission characteristics of the emitting protrusion and which are power density dependent can be considered. One possible mechanism would involve the emission of photons by bombarding electrons which could be returned to the cathode and cause the emission of photoelectrons. The current in the gap after n such cycles can be written as $I_n = I_o K^n$ where I_o is the initiating current, and K is some constant obtained by finding the maximum number of photons N_p emitted per incident electron at the anode under all possible conditions and of all possible wavelengths and multiplying by the maximum number of electrons N_e emitted per incident

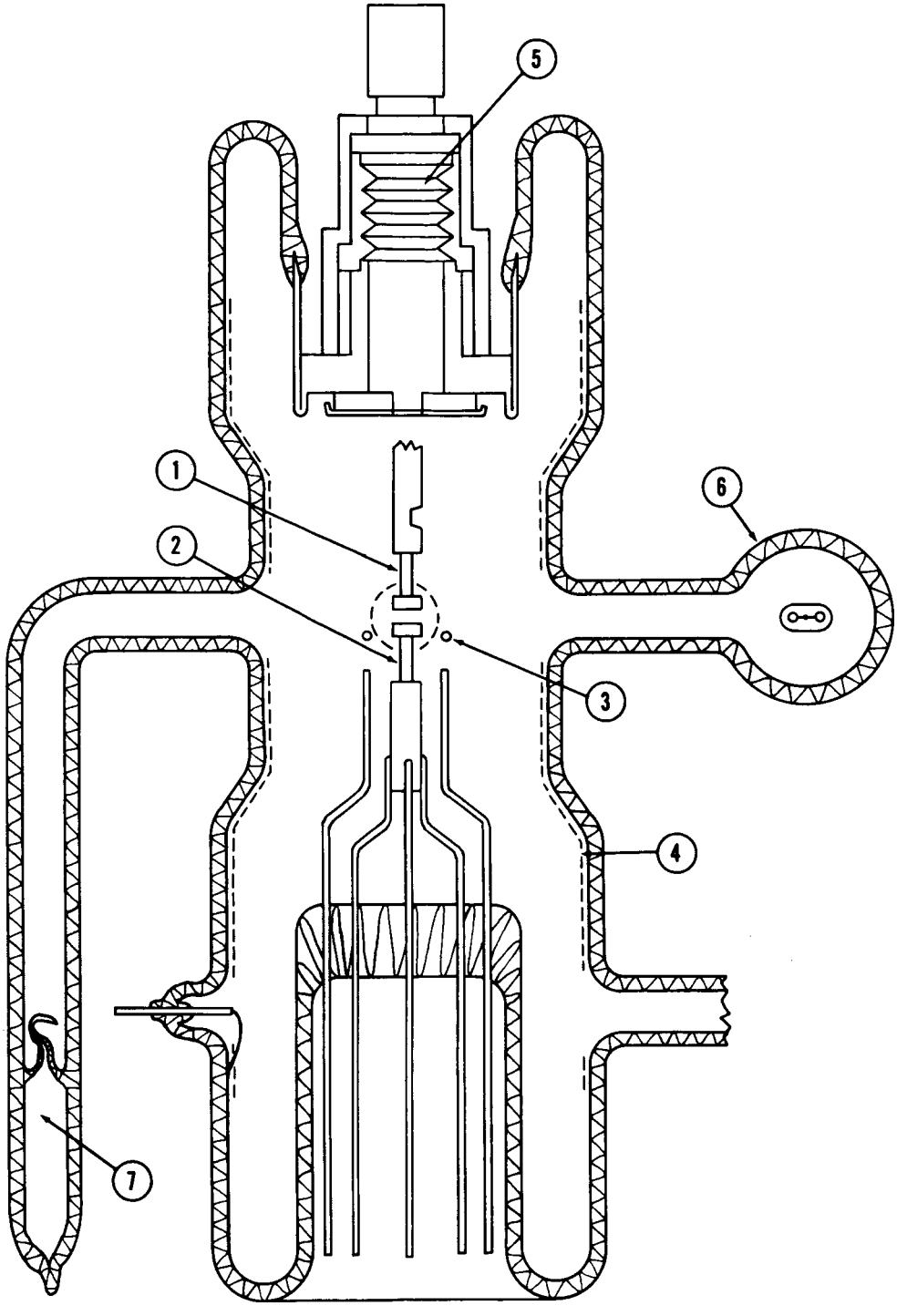

Figure 1. Variable gap spacing copper-tungsten diode with the following features: 1) 200 mil diameter disk that is 75 mils thick attached to a 60 mil diameter rod; 2) identical copper electrode; 3) outgassing ring; 4) stannous oxide conductive coating; 5) bellows assembly; 6) field emission microscope and 7) cesium source.

photon at the cathode under all possible conditions, i.e., $K = N_p N_e$. It can easily be seen that the condition for which the current will increase regeneratively is $K > 1$. From earlier work[5] the maximum number of photons per incident electron due to transition radiation is $\sim 10^{-4}$ and the maximum number of photoelectrons ejected at this frequency is $\sim 10^{-4}$, thus $K \sim 10^{-8}$ for this process. Another possible source of photons would be the production of x-rays from the impinging electrons, however, the yields would probably be quite low in the voltage range investigated, so that very probably K for this process would also be less than one. Since the efficiency of production of x-rays is directly proportional to the atomic number of the target material, the significance of photocurrent due to higher energy photons would be greater for tungsten or even molybdenum than for copper or aluminum. Some possible comparisons might be made by using other electrode materials.

For a voltage pulse length t_o that is greater than the time t_1 required for the anode to reach its steady state temperature, the I-V characteristics for a given electrode surface should simulate the d.c. condition. According to the theory presented in the last quarterly[2] breakdown should be anode initiated when the pulse length is very long compared with t_1 unless the surface enhancement factor γ is very large. As the pulse length is shortened the boundary value of the enhancement factor γ_o is lowered until the probability of a cathode initiated arc becomes greater than that of an anode initiated arc. In order to obtain experimental verification various values of pulse length were used with varying degrees of surface roughness. Fowler-Nordheim plots of some of the results are shown in Figures 2 and 3 where the curves of Figure 2 are from clean molybdenum at various spacings and γ, while those of Figure 3 are from heavily cesium-covered molybdenum electrodes. Curve 1 of Figure 2 shows the I-V data from a surface with an enhancement factor of 18.4 corresponding to a conical protrusion of tip radius $R_c = 5.5 \times 10^{-6}$ cm. For this surface an anode initiated breakdown would be expected since $t_o/t_1 = 3.8$ and γ is much less than γ_o. Curves 2 and 3 of Figure 2 are for surfaces whose enhancement factors are approximately equal (72 and 71 respectively). However, $t_o/t_1 = 1.43$ for curve 3 and $t_o/t_1 = 11.1$ for curve 2. The deviation from linearity of both these curves and for curves 2 and 3 of Figure 3 is due to electron space charge effects, which are quite significant when current densities are high.

The curves of Figure 3 were obtained from a surface heavily cesium coated. The value of t_o/t_1 for curve 1 was only .265, thus the anode was not able to reach its steady state temperature. However, the enhancement factor for this surface was 10, which is still below the value of $\gamma_o = 50$ so that the theory would predict an anode process to initiate the arc. Unfortunately, the cesium coverage was found to decrease during the pulse interval, making temperature calculations unreliable. Curve 2 of Figure 3 shows the Fowler-Nordheim plot for a surface whose enhancement factor was 47.8, while curve 3 shows the reproducibility of the data points of curve 2.

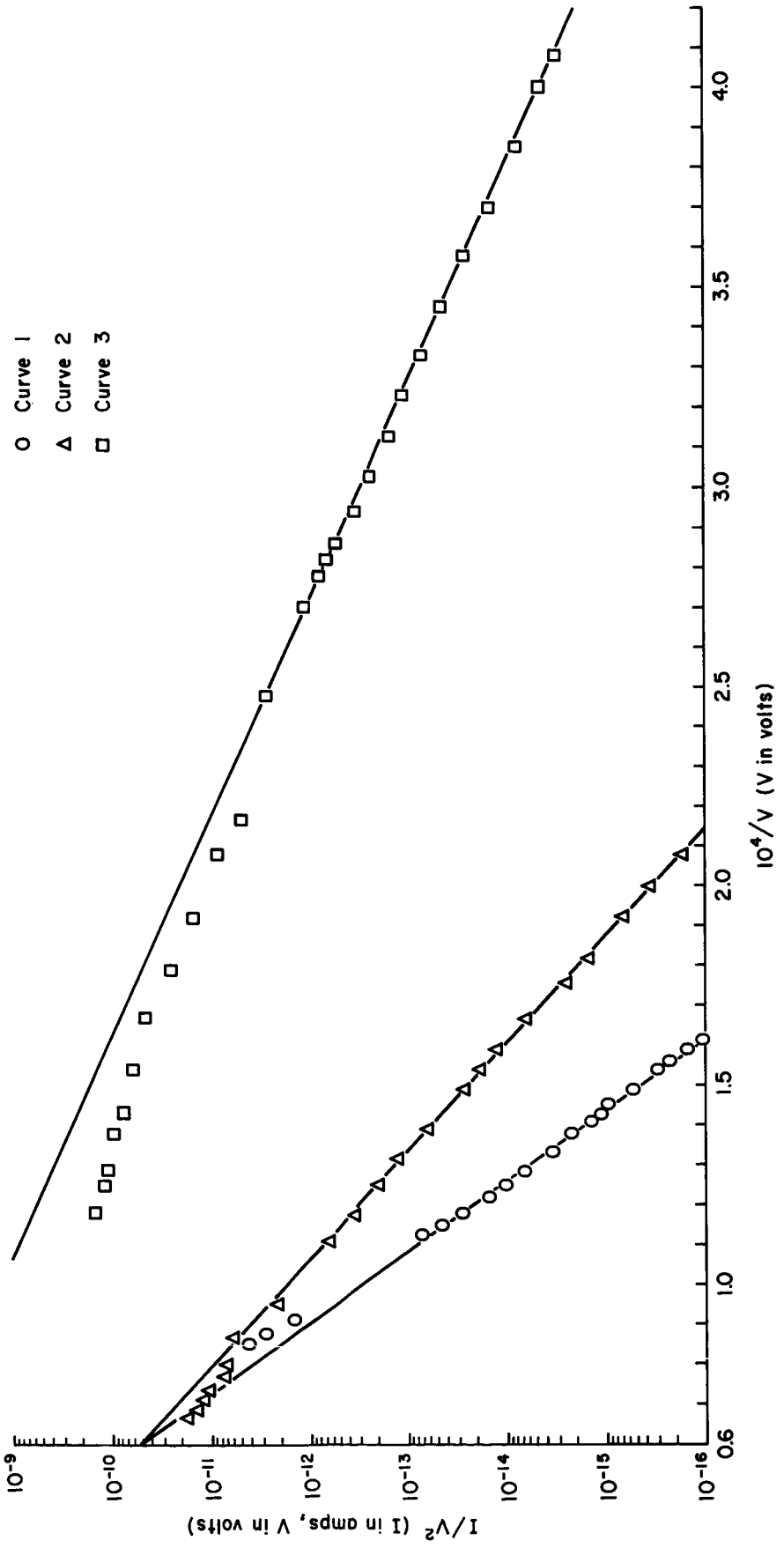

Figure 2. Fowler-Nordheim plots of I-V data from clean molybdenum electrodes with various amounts of surface roughness, and several different gap spacings.

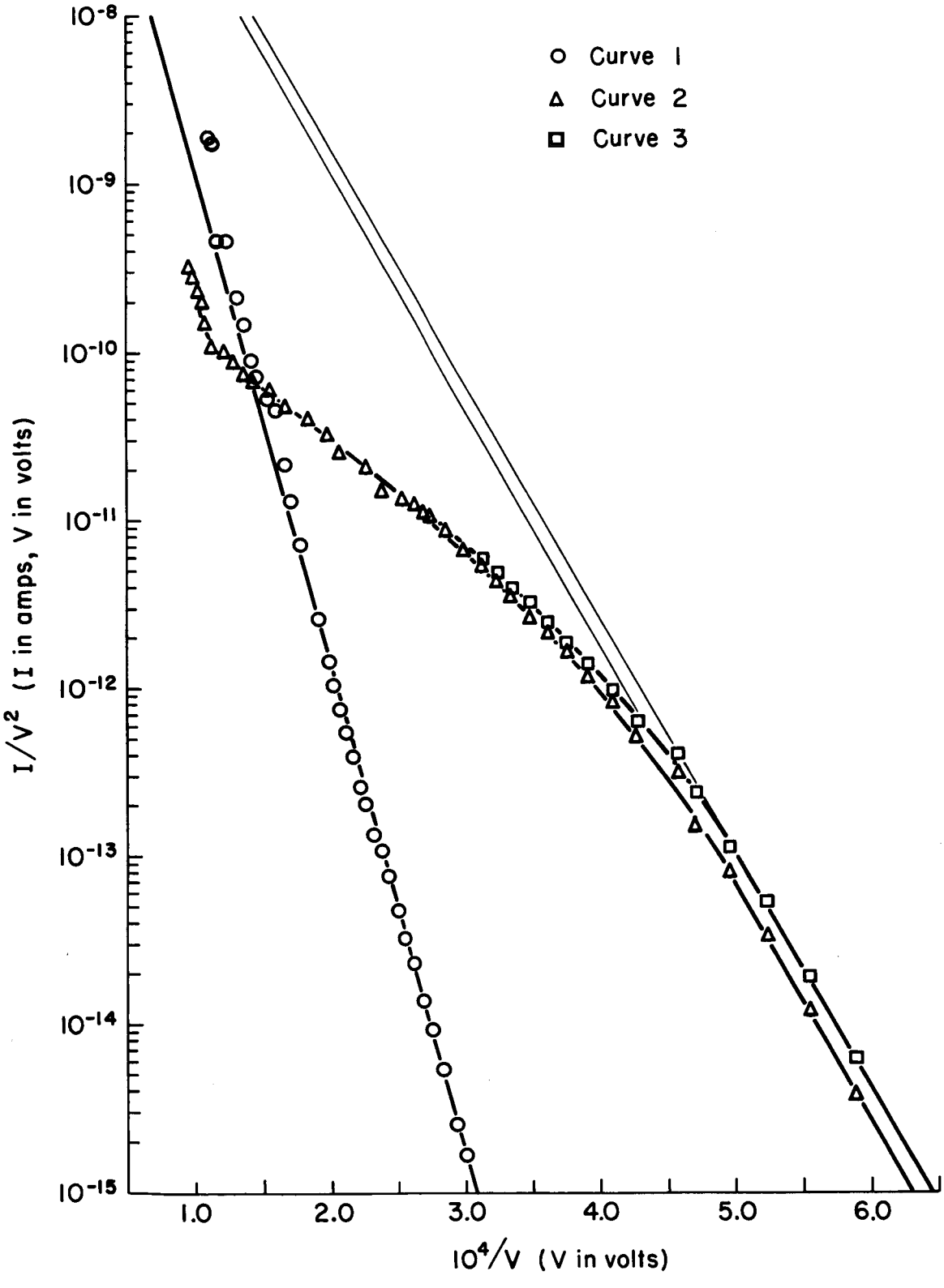

Figure 3. Fowler-Nordheim plots of I-V data from cesium-covered molybdenum electrodes (ϕ = 1.4) at different gap spacings and for two different values of enhancement factor.

On the basis of the theory presented in the last quarterly report one would predict an anode initiated arc for all cases in the above data except that shown in curve 3 of Figure 2. The results of analyzing the pulsed voltage data showed that the cathode current density J_c at which breakdown occurred followed trends listed below indicating agreement with theory.

At constant γ:

J_c decreased with increasing pulse length t_o

J_c increased with decreasing t_o

At constant pulse interval t_o:

J_c decreased with decreasing γ

J_c increased with increasing γ

In attempting to calculate temperatures at the anode from J_c, however, it was found that the numbers were unreasonable. For example, the calculated anode temperatures for the data of curves 2 and 3 of Figure 2 were in excess of 10^4 °K. Although the theory does take into account the field distortion around the emitting protrusion due to the close coupling of the emitter with the supporting planar surface upon which it sits, it does not take into account the influence of either ion or electron space charge which must be present just prior to the arc at high emission densities. Since the reproducibility of the data points up to the arc as shown in Figure 3 indicates that there were no significant ion currents, it is interesting to examine the effect of the electron space charge.

Early in the development of field emission technology it was noted that as the electric field at the tip of a field emitter became very large, the current increased less rapidly with increasing voltage than the Fowler-Nordheim theory would predict. This was not due to a failure of the theory, but to the onset of space charge effects. The space charge in the beam increases with increasing current and causes the electric field actually present at the emitter surface to be less than the calculated field βV by an amount that increases with increasing emitted current. As a result, space charge can have significant effect because of its magnitude at high current densities.

The need for a knowledge of field emission characteristics at high emission levels led to an early study of space charge effects by personnel of this laboratory[6], followed by a later and more detailed study[7]. The problem was analyzed by looking for solutions to Poisson's equation with the proper boundary conditions for the field emission diode. The resulting equations could not be integrated, thus certain geometrical approximations had to be made. Careful study of the problem showed that the best approximation to the potential distribution along the axis of a field emission

diode would be that of a cylindrical diode having the same cathode radius r_o, the same cathode field F_o and the same cathode-anode spacing d. The resulting equation which gives the desired solution for space charge limited field emission is:

$$F_1^2 V_o - F_1^3 r_o \ln \frac{d}{r_o} = \frac{4}{3} k J_1 V_o^{3/2} - 3k^2 J_1^2 r_o^2 \ln^2 \frac{d}{r_o} \qquad (2)$$

$$J_1 = A F_1^2 e^{-\frac{B}{F_1}} \qquad (3)$$

where $k = 1/\epsilon_o \sqrt{m/2e} = 1.9 \times 10^5$ volt $^{3/2}$/amp

J_1 is emitted current density

F_1 is the cathode field

V_o is the voltage applied (V = 0 at the cathode)

As the value of J_1 increases, F_1 decreases, however, J_1 cannot increase beyond the limiting value of J_s for which the right hand side of equation (1) and therefore also the cathode field vanishes.

$$J_s = \frac{4}{9k} \frac{F_o^{3/2}}{r_o^{1/2}} \frac{1}{(\ln d/r_o)^{1/2}} \qquad (4)$$

The limiting current density J_s is fully determined by the emitter radius r_o, the cathode-anode spacing d and the electric field $F_o = \beta V_o$ that would exist at the cathode surface in the absence of emission.

In Figures 4 and 5, the data of Figures 2 and 3 are plotted with the emitted current density as a function of the electrostatic field. In order to calculate the value for J_s shown in these figures, a value must be given to r_o, the apex radius of the emitting protrusion. To calculate r_o from the low J prebreakdown data and the relationship I/J = A, some relationship between A and r_o must be established. The effective emitting area is not really constant but increases as the anode voltage increases due to the non-linearity of the field emission response and because of the onset of space charge effects which occur first near the protrusion apex where field and emission are greatest. However, if the effective emitting area is expressed as $A = \lambda r^2$ where λ is constant for a given field, it can be shown[7] that λ ranges from 1 to 4 for clean tungsten when the electrostatic field F is between 30 and 100 Mv/cm. Using the value of A and λ from the low J prebreakdown data, a value of r_o can be calculated which will be constant for all values of J and F. For most values of field and current density, $\lambda \sim 2$. Using this average value and assuming that the effective emitting area is constant for all values of current density investigated, curve 1 of Figure 4

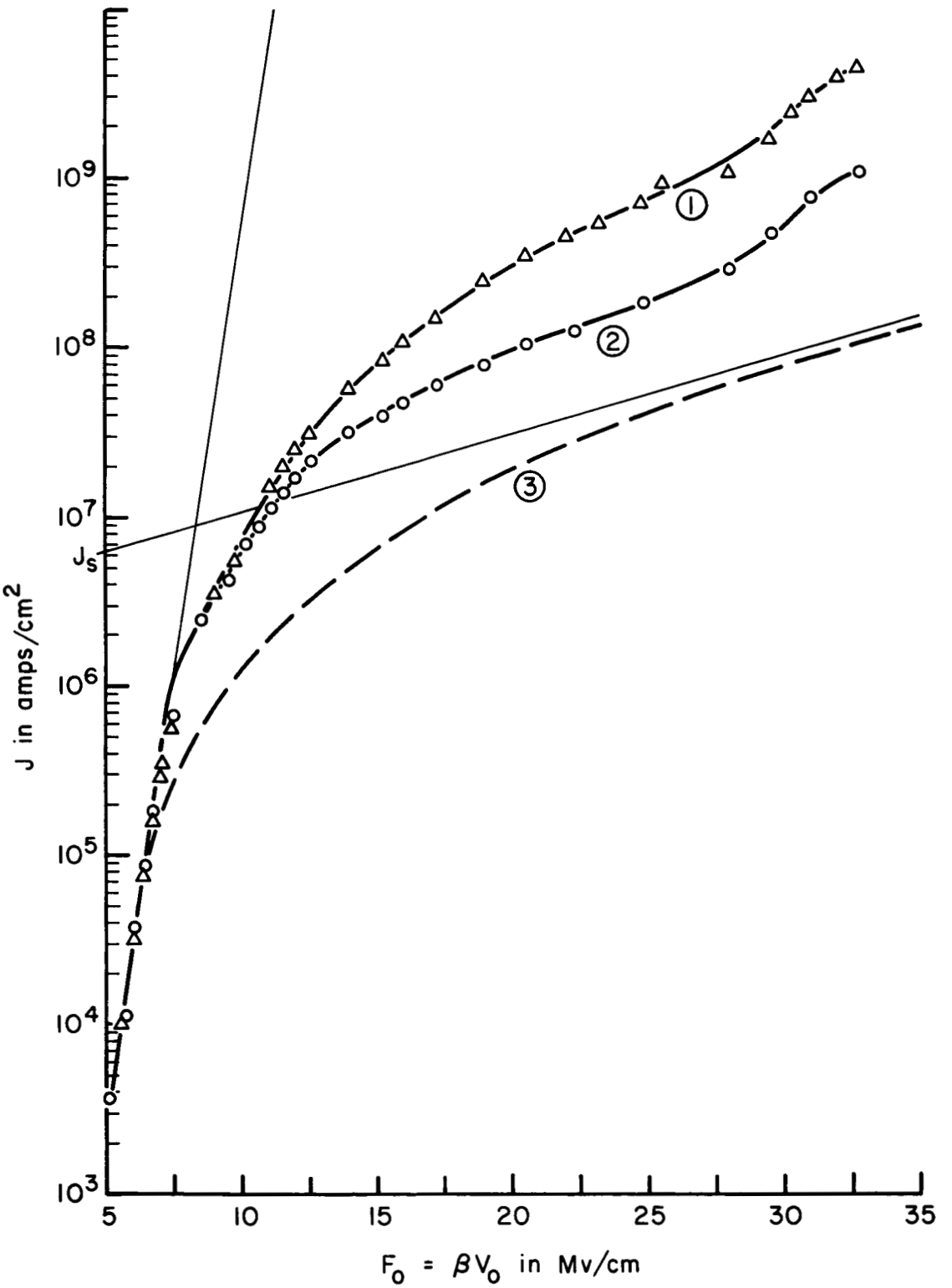

Figure 4. I-V data of Curve 2, Figure 3 plotted as current density J = I/A vs. electrostatic field at the protrusion tip F_o. Curve 1 shows the experimentally recorded values of current divided by the emitting area calculated from the low current density I-V data. Curve 2 shows the same data except that the effect of field and current density have been taken into account in calculating effective emitting area. Curve 3 is the predicted curve if only the original protrusion emits.

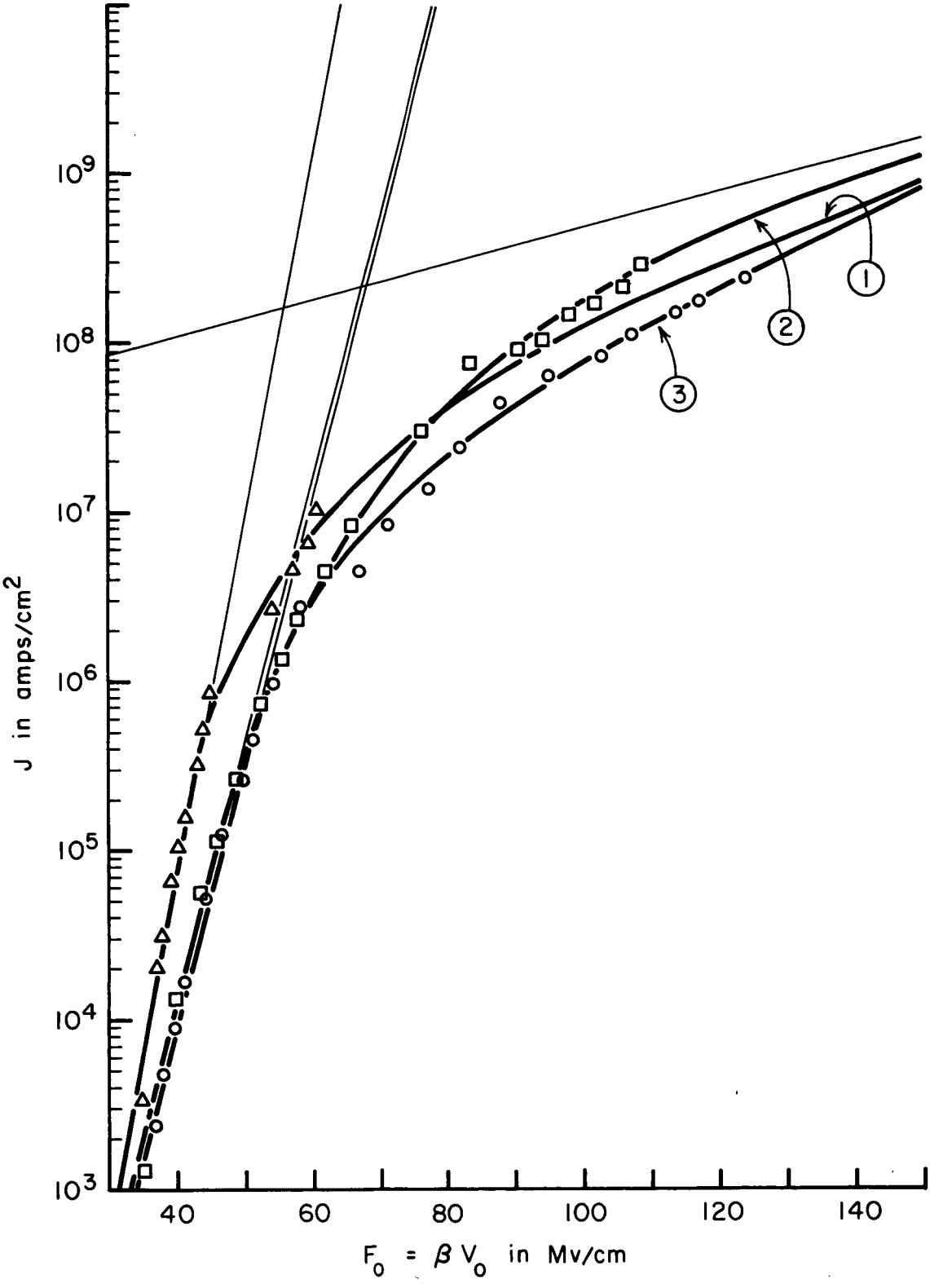

Figure 5. Shows current density as a function of electrostatic field using the clean molybdenum data of Figure 2. The curve numbers correspond to the respective curve numbers of Figure 2.

can be obtained for the current density as a function of electrostatic field. If the effect of changing emitting area is considered, the values for current density will be those shown in curve 2. It can be seen that in the low J region, the two curves are essentially the same but that there is a considerable difference as the current density increases. The effect of field on effective emitting area is taken into account when calculating the values of J shown in Figure 5. It is immediately obvious from Figure 4 that the values of J are much too high even when the effect of changing emitting area is taken into account when cesium is on the surface. Thus with cesium present and when the value of γ is high, it seems most likely that as the originally most highly emitting protrusion attains a current density sufficient for a large electron space charge region to form just in front of its apex, emission from this protrusion is suppressed so that it does not become thermally unstable before other protrusions with slightly lower γ are capable of contributing significantly to the total emitted current. Since space charge effects are observed at lower values of J for surfaces with lower work function, one would expect the experimentally observed space charge effects and the occurrence of much higher total currents without an arc for low ϕ surfaces.

At the cathode the electron space charge is a contributing factor at high current densities in increasing the effective emitting area, thus the value of current density will be lower than that calculated by assuming that the emitting area remains constant. Since the temperature at the tip of the emitting protrusion is proportional to the square of the current density, the calculated temperature of the emitting protrusion can be too high by a factor of between 4 and 16 depending on what is assumed to be the constant emitting area if the space charge effect is not taken into account.

In order to see what effect the space charge at the tip of a protrusion will have on the current density at the anode, a calculation must be made to determine how much beam spreading there will be at a distance from the emitter d equal to the gap spacing since $d \gg h$ where h is height of the protrusion. A rough approximation can be made by referring to an analysis of the beam spreading in a circular electron beam between parallel planes due to electron space charge repulsion. If space charge effects are neglected, at a distance d the radius of an electron beam emitted from a cylindrical protrusion of apex radius r and height $h = \gamma r$ that is sitting on one of two parallel plates a distance d apart can be expressed as[1]:

$$R_a = 2\sqrt{\gamma r d} \qquad (5)$$

This expression takes into account the compression of the beam caused by the close proximity to the emitting apex of the supporting plane. The approximations made in deriving equation (5) are the following[8]:

1) The protrusion has a particular geometry, that of a hemispherically capped circular cylinder with its axis of symmetry perpendicular to a plane where the plane is a distance d from a second parallel plane.

2) The electrons emitted from the hemispherical cap move with a radial velocity component v_r (radial in spherical coordinates centered at the protrusion) which can be calculated from the radial potential distribution of the protrusion, by taking the difference in potential at $r = r_o$ and $r = \infty$. Thus v_r is overestimated by taking the potential at $r = \infty$.

3) v_r is assumed to exist initially although it actually reaches its final value near the surface of the protrusion.

4) At some distance from the protrusion, v_r will be influenced by the parallel field causing the electron trajectory to become more parabolic.

If $\gamma \sim 100$ the approximations will be reasonably correct since v_r will be acquired over a fairly short distance.

Spreading of the beam due to space charge repulsion can be calculated according to an analysis of Vibrans[9] if it is assumed that at a distance of a few tip radii from the hemisphere the electron beam is circularly symmetrical about an axis perpendicular to the parallel plates and that in any plane perpendicular to the beam axis, the electrons are monoenergetic. From Vibrans' analysis one obtains a ratio r/r_o which is the ratio of the radius of the beam due to the electron space charge repulsion in the radial direction (where now the radial direction is in a direction parallel to the planes) r to the initial radius of the beam r_o. A rather crude approximation of the beam radius at the anode can be made by replacing the value of r in equation (5) by the above value of r and letting r be the radius of the emitting protrusion. This will underestimate the value of R_a since r_o should actually be chosen to be the radius of the beam a few tip radii from the surface of the emitter, however, perhaps this underestimate of R_a will partially compensate for the overestimate of R_a as given by equation (5).

The importance of considering space charge repulsion in the beam when calculating anode spot temperature ΔT_a can be seen in Table I where both the anode and the cathode temperatures are calculated for the arc conditions. Equation (1) was used to calculate the anode temperature. In order to calculate the cathode temperature, the following equation derived for a resistively heated field emitter[10,11] was used:

$$\Delta T_c = (9.5 \times 10^{-4}) J_c^2 r_o^2 \qquad (6)$$

TABLE I

Data	ΔT_c	ΔT_a (neglecting space charge)	ΔT_a (considering space charge)	γ/γ_o	t_1/t_o	d (mils)
Figure 5: (Clean Mo)						
Curve 1	5.7°K	2900 °K	885 °K	.332	3.8	1.4
Curve 2	404.0°K	1.38×10^{4}°K	1970 °K	.910	11.1	3.9
Curve 3	605.0°K	1.64×10^{4}°K	2480 °K	1.390	1.43	1.9
Figure 4 (Cs on Mo)	69.5°K	3.81×10^{6}°K	2620 °K	.960	.265	5.9

Copper-Tungsten Diode

A field emission initiated arc will occur when at least one of the electrodes has been heated to some critical temperature as defined in Equations (1) and (6). It seems reasonable to assume that this critical temperature must be related to the vapor pressure of the electrode material, since the critical temperature is that temperature at which sufficient electrode material can be evaporated into the gap that the probability of ionization occuring is significant. In order to gain a better understanding of the role of electrode temperature in determining arc conditions, a tube was designed in which one of the electrodes was made of copper and the other was made of tungsten. These two materials were chosen not only because of the wide spread in melting temperatures, (the melting point of copper being roughly one-third that of tungsten) but also because of the fact that the vapor pressure at the melting point of the two materials is almost two orders of magnitude lower for copper than it is for tungsten.

Measurements were made in an ambient helium pressure of $\sim 10^{-7}$ torr as determined by methods used previously at this laboratory[12] in which the deterioration time of the field emitter in an appendage microscope can be related to the pressure of helium gas in the tube through the empirical equation:

$$\frac{1}{I}\frac{dI}{dt} = 10^{11} P\, I^{0.75} \qquad (7)$$

where t is the time in hours, P the pressure in torr, and I the field emitted current at constant voltage. Since no change in current at constant voltage was observed for a period of time of 30 seconds, it was possible to use the appendage microscope by applying the voltage for only a few seconds at a time. Using this method it was determined that the pressure of other gases in the tube was $\sim 10^{-9}$. The adsorption of helium gas on either electrode is negligible so that the presence of this gas in the gap would not alter the

surface conditions by contaminating the electrode surfaces. However, the probability of ionizing the gas atoms by an electron beam is significant at these pressures as observed by the deterioration of the field emitter in the appendage microscope. If these ions are allowed to form they will sputter the electrode surfaces and change the shape of emitting protrusions. Thus by varying the length of time that the voltage is applied in the gap, the sputtering of the cathode surface can be varied from no effect (voltage applied for less than 30 seconds) to sufficient damage to cause an arc.

The information obtained from the tube showed that although the copper surface had a slightly higher enhancement factor (93 for the copper and 70 for the tungsten) the current density at breakdown when the voltage pulse was too short for significant helium ion sputtering to occur was much higher when the copper electrode was the cathode than when the tungsten electrode was the cathode. The theory would predict that for two electrodes of the same material the anode would initiate the arc. This means the observed behavior would be predicted, that is, the current density at breakdown would be lower when the copper electrode was the anode than when the tungsten electode was the anode.

By applying the voltage for a sufficiently long time the surface geometry of the emitting protrusion could be changed slightly due to helium ion sputtering. If the cathode was copper this damage would heal at room temperature after the field was removed, indicating that helium ion sputtering damage on copper can be removed at room temperature. By cooling the copper cathode to liquid nitrogen temperature the damage to the surface remained until the copper was heated. If the cathode were tungsten, this damage would not heal at room temperature in agreement with earlier reported sputtering work[2], where it was shown that sputtering damage of a tungsten emitter bombarded by cesium ions could be completely removed only after the emitter had been heated to 800°K, while only about 70% of the damage could be removed at room temperature. It is not unreasonable to assume that for copper whose melting point is one-third that of tungsten, the temperature required to remove slight amounts of sputtering damage would be one-third that required to heal a similar amount of damage on tungsten.

SURFACE KINETICS FOR METALLIC ADSORPTION

VARIATION IN WORK FUNCTION OF VARIOUS METALS ON CESIUM ADSORPTION

The average work function change as a function of cesium coverage was reported earlier[2] for cesium on tungsten and rhenium. Also, results were obtained for the variation of work function with cesium coverage on single crystallographic planes of tungsten, namely the (100) and (110) planes. These results have helped to provide a better understanding of the adsorption process, since they can be compared with available theoretical models more readily than results of measurements on polycrystalline surfaces which in some manner average large differences in local work function. During the past quarter, these results have been extended to include a measurement of the average work function change for cesium adsorption on molybdenum. These results coupled with early results on tungsten and rhenium provide data for the average work function change vs. cesium coverage for the three refractory metals: tungsten, molybdenum and rhenium.

Experimental Procedures and Results

The experimental procedures and method of obtaining the average work function vs. absolute cesium coverage were identical to those described previously[12]. This experiment was implemented by employing molybdenum and tungsten emitters side by side in the two-emitter tube and calculating the average coverage on the molybdenum emitter relative to that of the tungsten emitter by establishing the beam attenuation and knowing the emitter-to-source distances.

The procedure followed is to dose both emitters from a source in line with the two emitters and measure the work function of each emitter after the cesium has been spread to give an equilibrium coverage over the total emitter surface. The emitters are dosed while at liquid nitrogen temperature so that the assumption of a sticking coefficient of unity is valid; the surface migration is performed at temperatures sufficiently low that thermal desorption is negligible. The results given in Figure 6 show the ϕ vs. σ relationships for the three refractory metals which have been investigated. The data points are given for the most recent results on a molybedenum substrate.

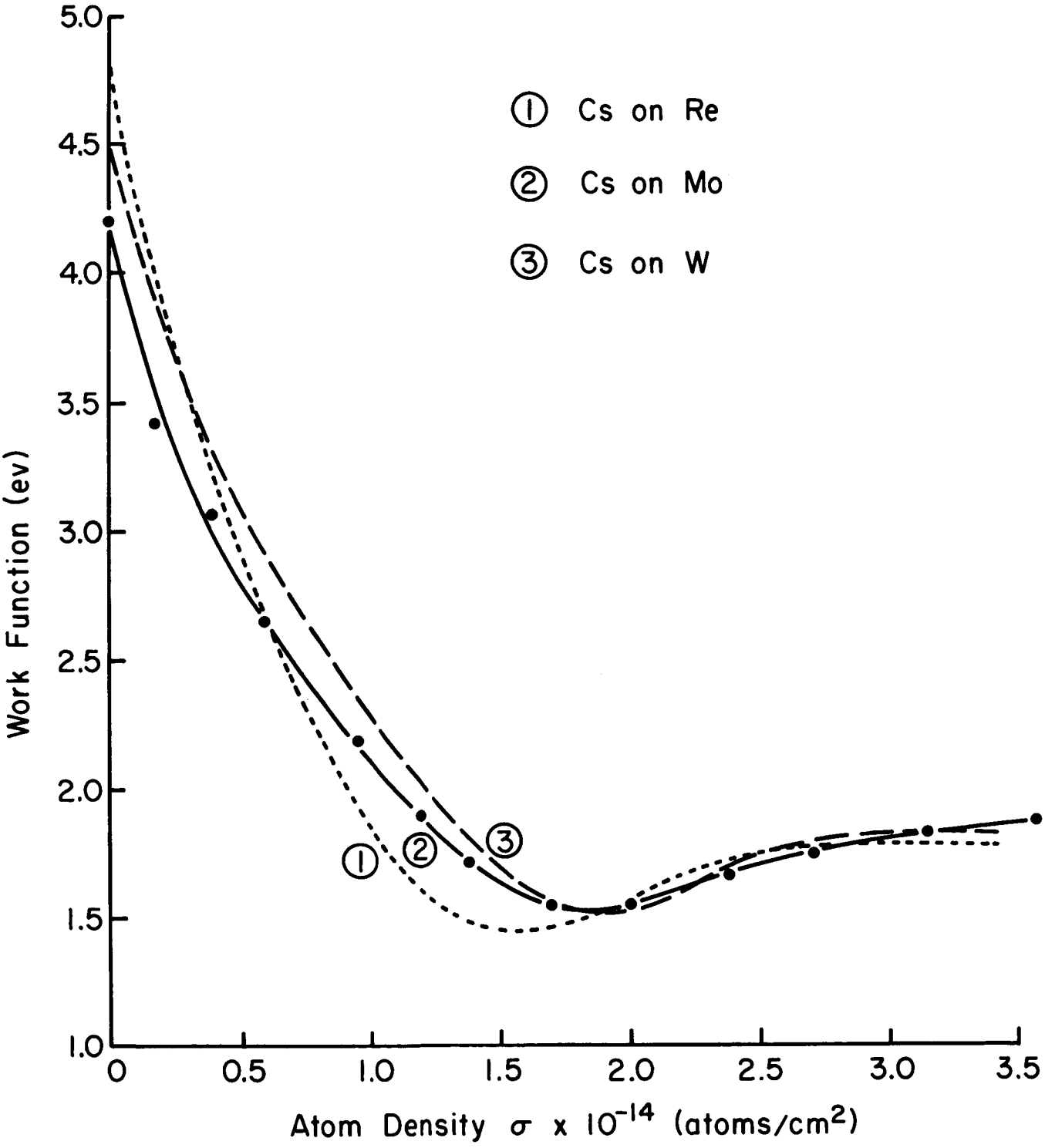

Figure 6. Two-emitter tube results of the work function vs. average cesium atom density on rhenium and molybdenum relative to tungsten.

Discussion of Results

It is interesting to note that the variation of work function with average cesium coverage shows a similar relationship on all three substrates. Within the accuracy of this measurement, which is probably within 10%, the coverage σ_m at which the minimum in work function occurs is the same for tungsten and molybdenum. This is not unexpected inasmuch as both possess body-centered cubic structures with near identical lattice constants. A summary of the salient features of the results such as the maximum work function change $\Delta\phi_m$, the minimum work function ϕ_m, and the value of work function at the highest coverage investigated, ϕ_o, are given in Table II.

TABLE II

Summary of maximum work function change $\overline{\Delta\phi}_m$ and work function $\overline{\phi}_o$ at $\sigma = 3.2 \times 10^{14}$ atoms/cm^2

Substrate	$\overline{\phi}_s$ (ev)	$\overline{\phi}_m$ (ev)	$\overline{\Delta\phi}_m$ (ev)	$\overline{\phi}_o$ (ev)
Mo	4.20	1.55	2.66	1.81
W	4.52	1.52	3.00	1.78
Re	4.85	1.45	3.40	1.82

Values of ϕ_m decreased slightly as the average work function of the substrate increased. An empirical relationship between the maximum work function change $\Delta\phi_m$ and the substrate work function ϕ_s, mentioned in a previous report[2], and which is of the following form

$$\Delta\phi_m = 1.09\,(\phi_s - 1.78) \text{ (ev)} \qquad (8)$$

appears to be obeyed by the above results. Inasmuch as earlier experimental results suggested anisotropies in the coverage distribution over the various exposed crystal faces, and in view of the strong reversal on emission of the (110) planes, one is not justified to utilize results of the above described nature to compare with theory. Instead, one must resort to the probe tube results in which work function changes are measured on single crystallographic planes.

MERCURY ADSORBED ON MOLYBDENUM

The changes in field emission pattern detail and in work function for adsorption and desorption of thin mercury films on a molybdenum substrate have been investigated by field emission techniques. Also, the activation energies for thermal desorption and surface diffusion of a low coverage of mercury on molybdenum were obtained from Arrhenius plots.

The behavior of mercury on molybdenum is found to be considerably different from that of cesium on molybdenum: (1) adsorption of mercury on molybdenum increases the work function rather than decreasing it; (2) a heavy coverage of mercury on molybdenum is mobile even at 77°K; (3) the high fields required for pulsed field emission (about 40 Mv/cm in this case) cause arcs to occur in the region of the emitter tip when it is covered with several monolayers of mercury. In connection with this latter point an arc is found to remove some of the adsorbed mercury from the emitting portion of the tip even though the tip is at a temperature of 77°K. For this reason the field emission patterns for mercury on molybdenum were photographed using dc electric fields, which are not as high as those required for pulsed operation.

Adsorption and Diffusion

Adsorption of mercury on molybdenum has been studied by two different methods, the first consisting of a series of successive doses with no thermal equilibration, and the second being a series of successive doses each being thermally equilibrated.

The results of the first method are shown in Figure 7, which is a series of field emission patterns taken during evaporation of mercury onto a molybdenum field emitter held at a temperature of 77°K. Figure 7 (a) is the emission pattern of clean molybdenum; Figure 7 (b) identifies the principal planes in the emission pattern. Figure 7 (c) was taken after the tip had been dosed with an amount of mercury chosen to be a unit dose N = 1. The darkening of the upper portion of the pattern by the adsorbed mercury shows that (1) mercury adsorbed on molybdenum raises the work function, and (2) for this particular degree of coverage mercury is not mobile on molybdenum at 77°K. Figure 7 (d) indicates that doubling the amount of mercury does not change the basic behavior of the mercury film. The uniform appearance of the pattern in Figure 7 (e), taken after dosing the tip a total amount N = 4, shows that at this higher degree of coverage mercury is mobile, even at 77°K. From this it may be inferred that N = 4 corresponds to a coverage greater than a monolayer, since multilayer

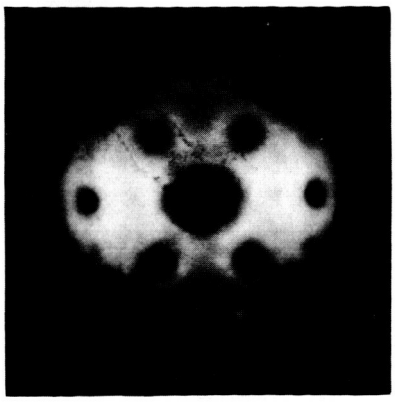

(a)
Clean Mo
ϕ = 4.20 ev

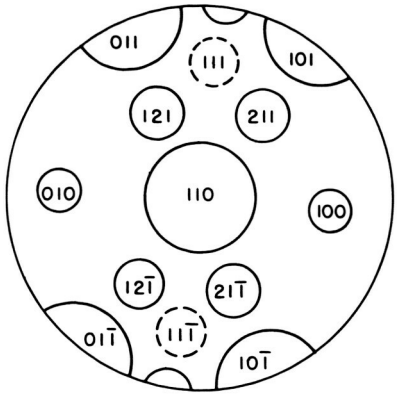

(b)
Principal planes of
(110)-oriented Mo

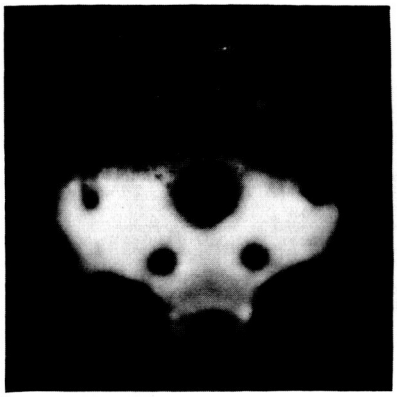

(c)
N = 1 (arbitrary units)

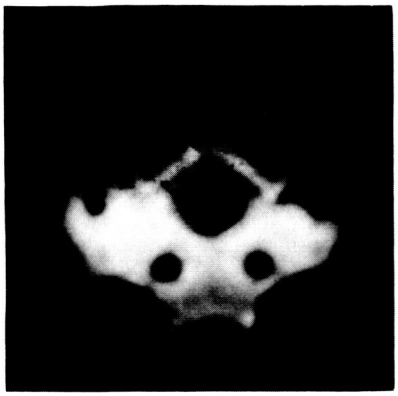

(d)
N = 2

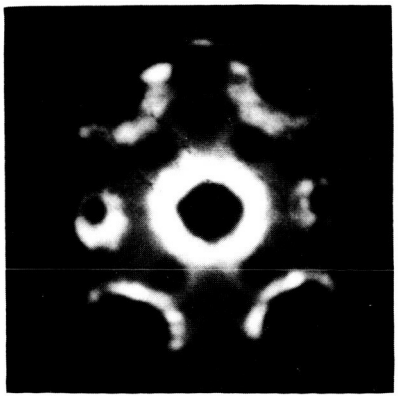

(e)
N = 4

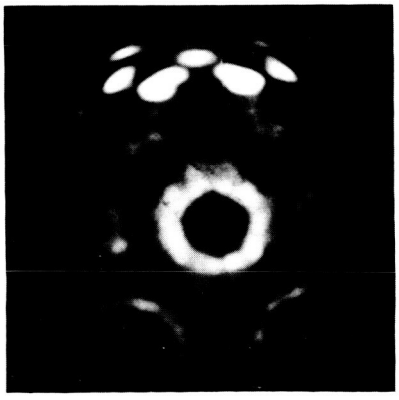

(f)
N = 6

Figure 7. Changes in the field emission pattern of a molybdenum emitter during adsorption of mercury. The relative amount of mercury on the emitter is given by the quantity N.

diffusion generally can occur at lower temperatures than first layer diffusion for most systems. The spots in the top of the pattern in Figure 7 (f), taken after dosing the tip a total amount N = 6, are indicative of mercury atom clustering, and suggest that epitaxial growth studies could be made on this system. Dosing a total amount N = 8 caused no further changes in the field emission pattern. Thus mercury was found to raise the work function when adsorbed on molybdenum and to be mobile in the second layer but not in the first at 77°K.

In the second method, the molybdenum tip was dosed with a small amount of mercury, which was then equilibrated over both the emitter tip and shank by surface diffusion. A photograph of the resulting field emission pattern was taken and the work function of the surface was determined from a Fowler-Nordheim plot. The results are shown in Figures 8 and 9. In Figure 8 are plots of the change in work function and change in log A, the pre-exponential part of the Fowler-Nordheim equation, as functions of the relative amount of mercury coverage. The maximum work function change is 0.42 ev, and in the opposite direction from the change caused by cesium adsorption on molybdenum. In a previous report[2] was stated an empirical relationship between ϕ_s the substrate work function, ϕ_a the adsorbate work function, and $\Delta\phi_m$ the maximum change in work function upon adsorption,

$$\Delta\phi_m = 1.09\,(\phi_s - \phi_a), \tag{9}$$

which was in good agreement with a number of adsorbate-substrate combinations. For mercury on molybdenum the above equation would predict a work function change of 0.35 ev, whereas 0.42 ev was actually measured; these two numbers are in reasonable agreement. However, for many other adsorbate-substrate combinations the work function change at the monolayer is very nearly equal to the contact potential between the bulk metals of the adsorbate and substrate, whereas it can be seen in Figure 8 that for mercury on molybdenum the work function drops below the adsorbate work function (4.52 ev)[14] and continues to drop with increasing coverage (the last point on the graph is of questionable validity because of the growth of projections on the emitter tip). Moreover, on another contract[15] the work function changes of mercury on tungsten have been measured; whereas equation (9) predicts zero change in work function for this system a work function change of 0.35 ev is actually measured. Thus at present the shape of the work-function/coverage curve for mercury on either molybdenum or tungsten raises more questions than it answers. Figure 9 shows the field emission pattern changes that occur during the adsorption run. In general the changes are quite small and the pattern looks rather similar to that of clean tungsten through most of the coverage range.

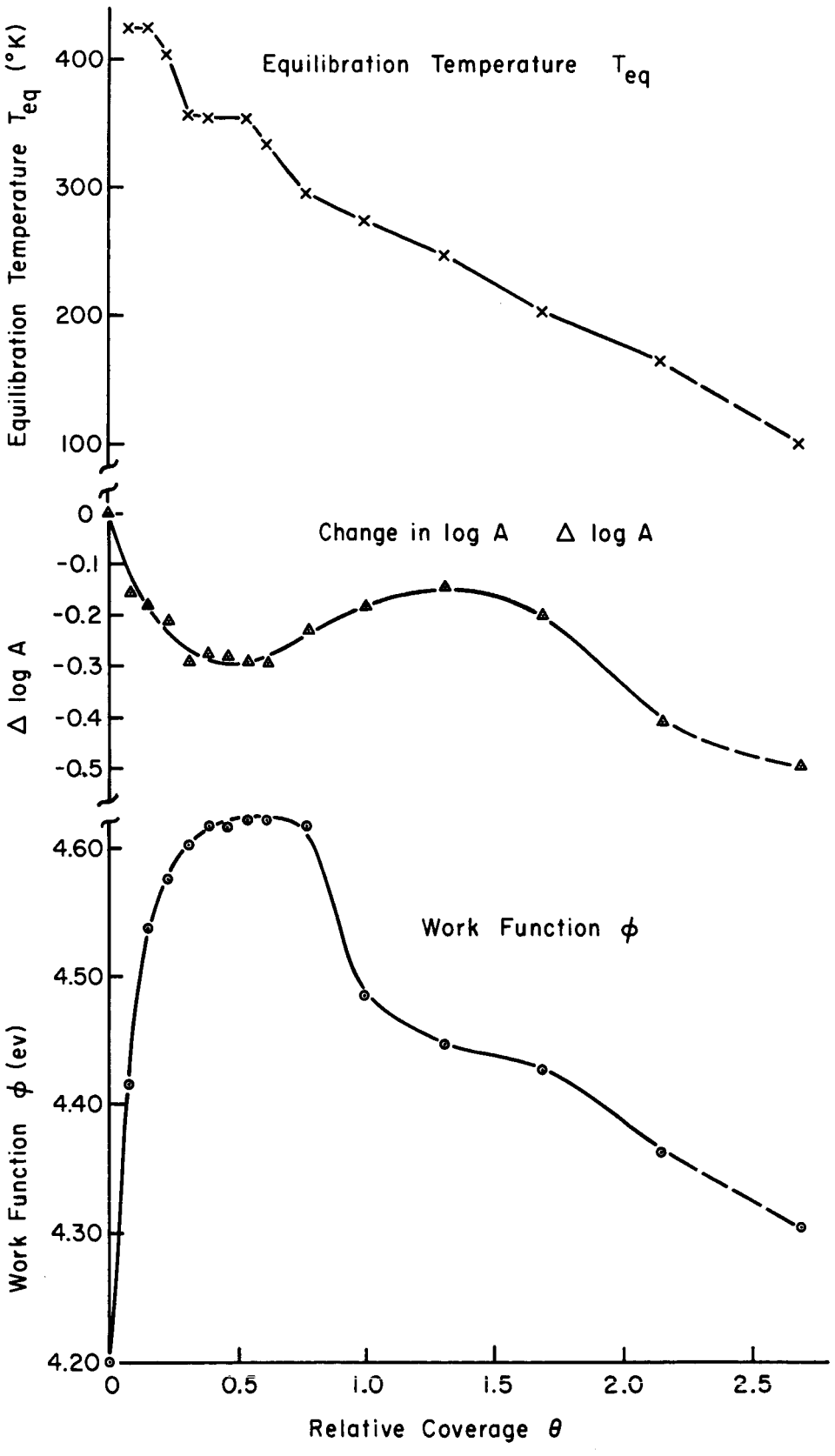

Figure 8. Changes in work function, the Fowler-Nordheim pre-exponential term A, and equilibration temperature as functions of the relative amount of mercury coverage for mercury on molybdenum.

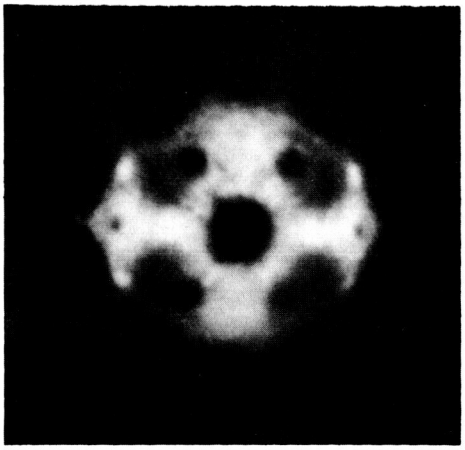

(a)
ϕ = 4.42 ev
θ = 0.08

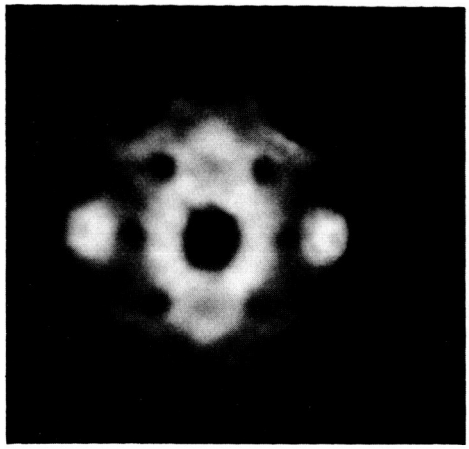

(b)
ϕ = 4.54 ev
θ = 0.15

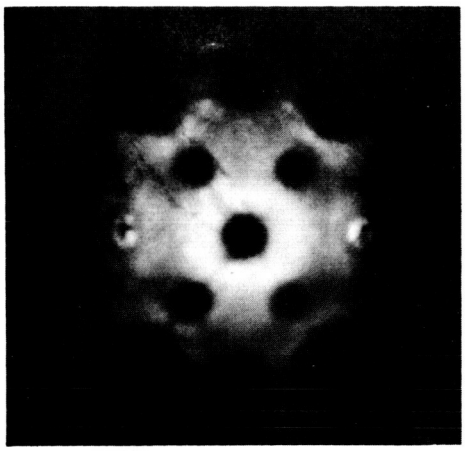

(c)
ϕ = 4.62 ev
θ = 0.77

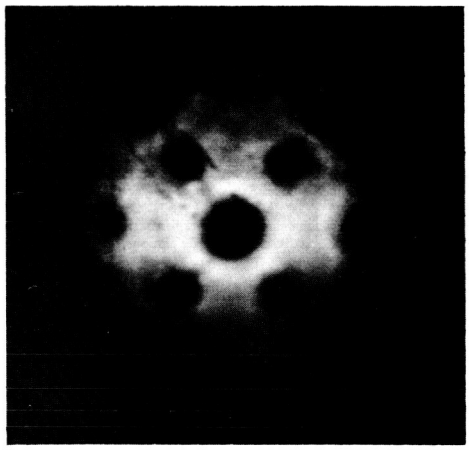

(d)
ϕ = 4.45 ev
θ = 1.31

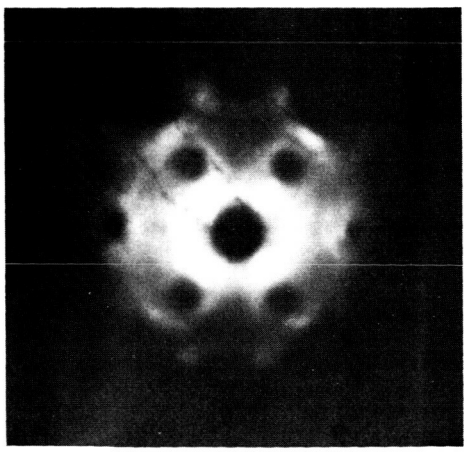

(e)
ϕ = 4.43 ev
θ = 1.69

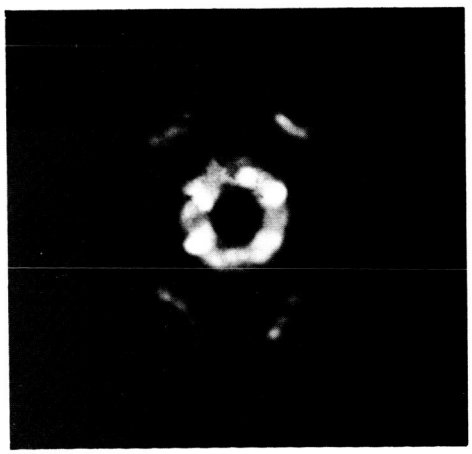

(f)
ϕ = unknown
θ 3.3

Figure 9. Field emission patterns for various coverages of mercury on molybdenum, after equilibration. The relative amount θ is based on the coverage scale of Figure 8.

Also plotted in Figure 8 are the temperatures required for equilibration of the various coverages over both the emitter tip and shank. This graph of equilibration temperature vs. coverage gives a rough idea of the change in diffusion constant as a function of coverage.

At a high coverage (greater than 2.5 on the relative coverage scale of Figure 8) viewing fields of 25 Mv/cm or greater were observed to cause the growth of projections near the edges of the {110} planes (the bright spots in the bright rings surrounding the {110} planes in Figure 9 (f)). When the viewing field was reduced to zero the projections (i.e., the bright spots in the emission pattern) disappeared, apparently due to the mobility of mercury at this coverage at 77°K. The projections could be made to grow and disappear many times by having the viewing field alternately above 25 Mv/cm or at zero. The growth of projections as in Figure 9 (f) is probably due to the electrostatic stress of the applied viewing field acting upon the mobile mercury layer and pulling mercury atoms toward points of highest field.

Thermal Desorption

The thermal desorption characteristics of mercury on molybdenum were determined in the usual manner; that is, the emitter was heated for 60-second periods to successively higher temperatures, and after each heating period was returned to a temperature of 77°K at which a photograph of the emission pattern was taken and the work function determined from a Fowler-Nordheim plot. The changes in work function are plotted as a function of desorption temperature in Figure 10. By using the work-function vs. coverage curve of Figure 8 a relation between the desorption temperature and relative coverage may be obtained; this is plotted in Figure 11. The desorption temperature is roughly proportional to the desorption activation energy; thus Figure 11 is essentially a graph of the variation of the desorption activation energy with relative coverage. The sequence of patterns obtained during desorption are the same as for adsorption but reversed; this indicates that the adsorption and desorption processes are reversible.

Diffusion and Desorption at Low Coverage

The activation energies for surface diffusion and thermal desorption of mercury from molybdenum have been determined from Arrhenius plots for the coverage interval 0 - 0.07 relative monolayer (that is between the coverages indicated by Figures 7 (a) and 9 (b)). The Arrhenius plots were obtained from measurements of the time required to go between two pulsed current measurements corresponding to the coverages indicated as a function of temperature. The results are shown in Figure 12. As would be expected, the desorption activation energy is less than the corresponding value for cesium on tungsten; however, the diffusion activation energy is considerably higher than for cesium on tungsten[16]. From the diffusion activation

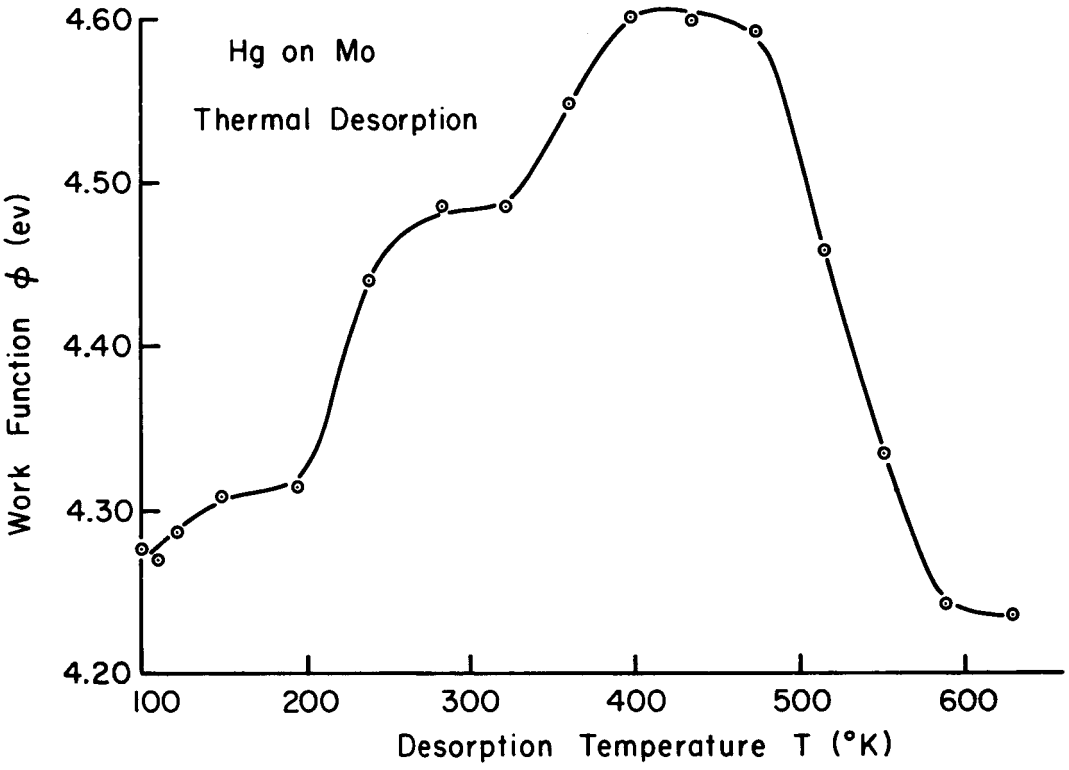

Figure 10. Work function of mercury on molybdenum as a function of desorption temperature to which the emitter had been heated for successive 60-second heating periods.

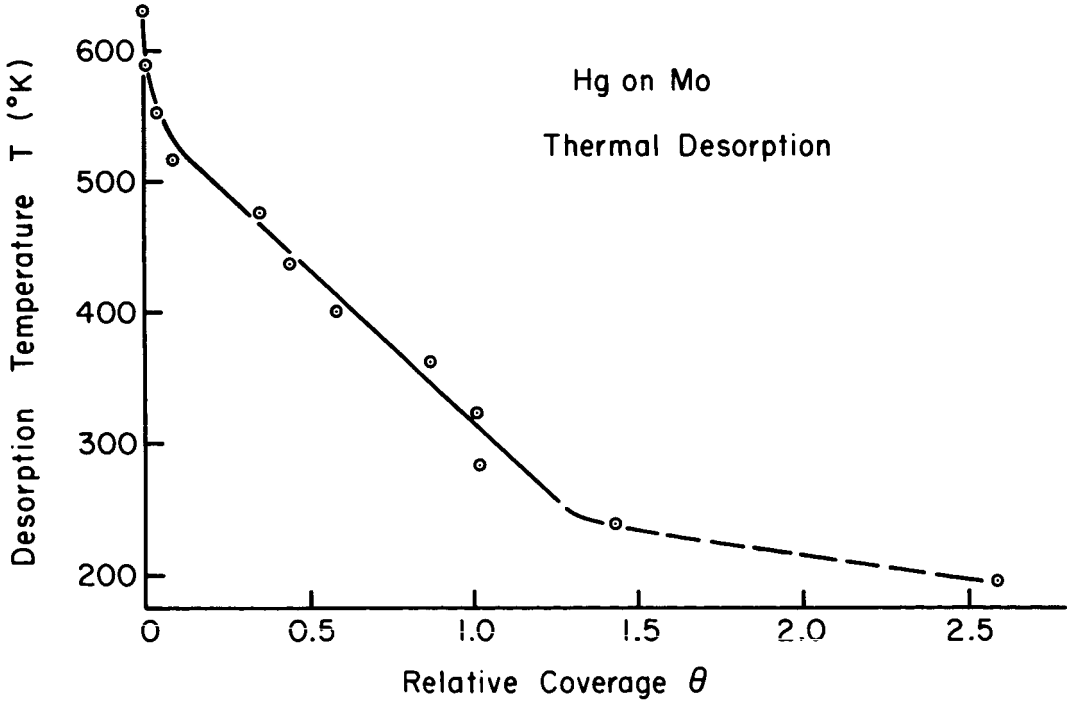

Figure 11. Desorption temperature for successive 60-second heating periods as a function of mercury coverage for mercury on molybdenum. The relative amount θ was obtained by means of Figure 8.

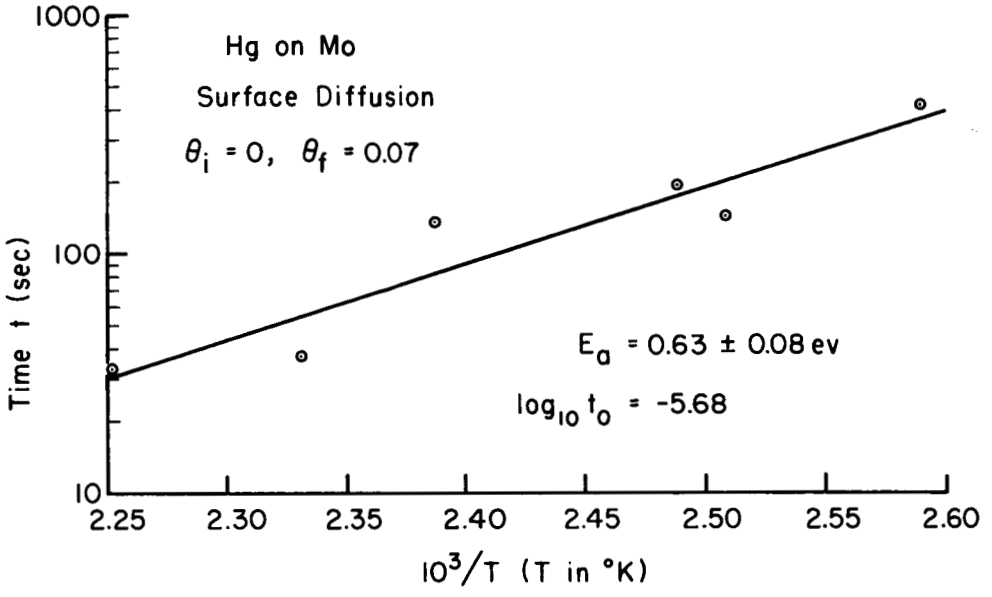

(a)

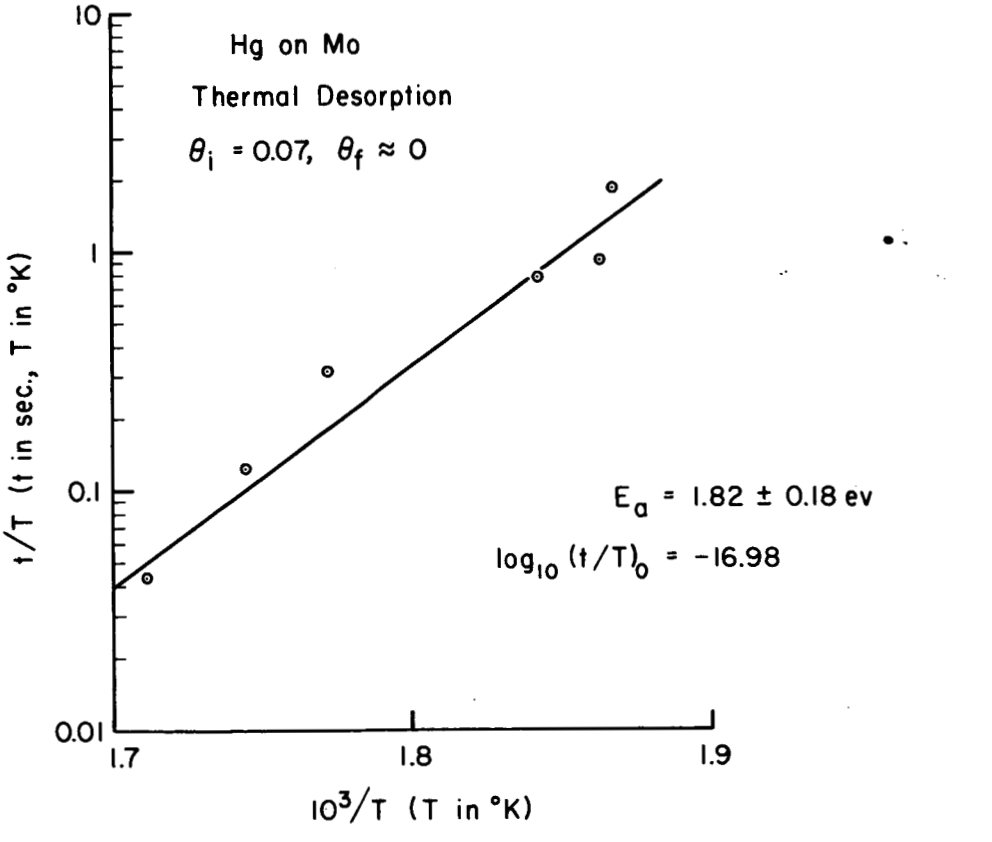

(b)

Figure 12. Arrhenius plots for a low coverage of mercury on molybdenum.
(a) Surface diffusion between coverages $\theta_i = 0$ and $\theta_f = 0.07$
(b) Thermal desorption between coverages $\theta_i = 0.07$ and $\theta_f \approx 0$.

energy and intercept the value of the diffusion constant D can be calculated for any temperature; for a temperature of 441°K and assuming a diffusion distance of 0.02 cm, D is equal to 1.0×10^{-5} cm^2/sec. With this information the equilibration temperature vs. coverage in Figure 8 may be converted into a graph of the logarithm of the diffusion constant vs. coverage.

STUDIES OF ELECTRONIC INTERACTIONS WITH ADSORBATES ON TUNGSTEN

Interest in the interaction of electrons with adsorbed layers is increasing at the present time due to such possible applications as electron-enhanced ion emission, production of clean surfaces by low energy electron bombardment, and others. So far, investigations of this nature have been performed primarily on electro-negative adsorbates. For these systems electron-induced desorption is thought to be caused by electron excitation of the localized adsorbate bond into an ionic or excited neutral state, leading to desorption of the ad-atom as an ion (or as a neutral if electron interchange between the adsorbate and substrate is sufficiently rapid). Studies made thus far[17,18] indicate that electron-induced desorption of electro-positive adsorbates is not likely, because of the delocalized nature of the metallic bond and the very rapid transition of electrons between the ad-atoms and the Fermi sea of the substrate. One recent measurement[17] of the system of barium on tungsten confirms this, since no measurable desorption was detected. It was the intent of this investigation to determine what occurs during electron bombardment of a system with both electro-negative and electro-positive adsorbates co-adsorbed, such as cesium and oxygen on tungsten.

A tube for the investigation of electron interactions with cesium and/or oxygen adsorbed on tungsten has been designed and is discussed in earlier reports[2]. Results described herein will summarize the investigation of the interaction of 294-volt electrons with adsorbed cesium layers at a variety of temperatures and cesium coverages.

EXPERIMENTAL METHODS AND RESULTS

The tube utilized for this investigation contained a standard cesium and oxygen source and an electron gun which was capable of delivering a current density of 24×10^{-3} $amps/cm^2$ at the emitter tip at an accelerating voltage of 294 volts. The configuration of the tube was such that the current density characteristics of the gun could be precalibrated prior to insertion of the tip. In addition, the emitter faced the electron beam so that impingement occured nearly normal to the emitter surface. The detailed construction of the tube and calibration of the electron gun assembly are described in detail in a previous report[2]. This tube is also capable of measuring work function changes on single crystallographic planes, however, for this investigation only average work function changes were measured.

Prior to dosing the tip with cesium, the gun was run for several minutes to establish the level of contamination of the tip due to operation of the gun alone. It was discovered that one of the lens elements aperturing the electron beam slowly liberated an electro-negative gas (presumed to be oxygen) which established a residual contamination rate of the emitter and hence, a minimum level of sensitivity for the detection of the electron-induced desorption of cesium. The contamination of the emitter by the electron-induced electro-negative gas is sufficiently slow that running the beam for 100 seconds caused no detectable work function change of the emitter. Thus it was assumed that any changes in work function of the cesium layer during electron bombardment in the space of 100 seconds should be due to electron-induced desorption of the cesium layer.

The procedure followed for this investigation was to dose the tip heavily and, after equilibration of the cesium dose, a work function measurement was obtained; this was followed by electron bombardment for approximately 100 seconds and another work function measurement. The cesium layer was then thermally desorbed to a lower coverage and the operation repeated. At some of the lower coverages, the emitter temperature could be raised from 77°K to as high as 660°K during the electron bombardment to establish the presence of any temperature dependence of the yields of electron-induced desorption. The work function changes caused by the electron bombardment should be related to coverage changes from previously established relationships between work function and cesium coverage.

The results of this investigation are summarized in Table III for a bombarding electron beam at 294 volts and a current density of 24.03×10^{-3} amps/cm^2.

TABLE III

Summary of Electron-Induced Desorption of Cs on W for 294-volt Electrons at a Current Density of 24.0×10^{-3} amps/cm^2

Desorption Time (sec)	T(°K)	ϕ_i (ev)	ϕ_f (ev)	(σ_i atoms/cm$^2 \times 10^{-14}$)	(σ_f atoms/cm$^2 \times 10^{-14}$)
106	77	1.77	1.78	1.41	1.41
100	77	1.82	1.82	1.35	1.35
100	416	2.08	2.10	1.15	1.13
100	77	2.10	2.13	1.13	1.11
100	77	3.66	3.65	0.25	0.25
100	663	3.72	3.74	0.23	0.22

DISCUSSION OF RESULTS

The results of Table III show that throughout the coverage and temperature range, the interaction of 294-volt electrons with cesium layers for all intents and purposes is negligible. Maximum cross section for the electron-induced desorption of cesium from tungsten can be estimated from the following kinetic arguments. For a given cesium atom density σ, the following first order reaction for the rate of electron-induced desorption can be deduced

$$\frac{-d\sigma}{dt} = N_e b_c \sigma \tag{10}$$

where b_c is the desorption cross section in cm^2 and N_e the electron flux in electrons/cm^2/second. The above first order desorption equation can be integrated to yield the following expression for the cross section in cm^2:

$$b_c = \frac{3.68 \times 10^{-19}}{Jt} \log \frac{\sigma_i}{\sigma_f} \tag{11}$$

where J is the current density in amp/cm^2 and σ_i and σ_f are the coverage at times 0 and t, respectively.

From equation (11) and Table III it can be deduced that the cross section for electron-induced cesium desorption must be less than 6×10^{-22} cm^2. The somewhat larger change which occurred at 663°K is attributed to thermal desorption rather than electron-induced desorption. These results are in agreement with similar results obtained for barium on tungsten[17] and the general expectations of the existing theory of electron-induced desorption. In the case of metallic adsorption where $I - \emptyset$ is small, it has been postulated that binding involves almost wholly delocalized electrons[19]. In such systems, the barrier for tunneling to and from the adsorbate is highly transparent so that transition times are extremely short. In this case one would expect excited ionic or molecular states of the adsorbate bond formed by electron impact to be extremely short lived (less than vibrational frequencies) because of rapid electron exchange with the electrons within the Fermi sea. The results with cesium on tungsten seem to confirm this view since no desorption could be detected throughout the coverage and temperature range investigated.

It is not obvious from the existing knowledge what one might expect during electron bombardment in the case of cesium co-adsorbed with oxygen on tungsten. Experiments are now under way to investigate this system by the above described methods.

SPUTTERING STUDIES

Most of the effort in this area has been expended on the field ion microscope study of xenon ion sputtering of tungsten, and is reported below. The experimental tube used for the field emission microscope study of cesium ion sputtering of clean and cesium-coated tungsten has been redesigned to provide a uni-directional cesium ion beam of known current density and is now ready for operation; results from this study should be available in the near future.

FIELD ION MICROSCOPE STUDY OF XENON ION SPUTTERING OF TUNGSTEN

Xenon ion sputtering of clean tungsten has been investigated as a function of ion energy for three different energies, 100 volts, 500 volts, and 1300 volts. It seems pertinent to review the experimental tube design and procedure followed in this study before giving the results.

Experimental Tube and Procedure

The field ion microscope (FIM) used in this study was standard[20] except for the addition of a Xe ion gun and a Faraday cage ion collector assembly for measuring ion current density (Figure 13). The FIM was liquid N_2 cooled; thus the W anode tip used as the sputtering target was maintained at a temperature of 77°K in this study. In the ion gun Xe gas was admitted to the ionizing chamber where it was ionized by electrons constrained axially by a magnetic field. The 14.0 v accelerating potential supplied to the electrons permitted ionization of Xe, but not of most other gases (e.g., N_2, CO, H_2, etc.) likely to be found in the system.

The tube was mounted on a liquid N_2 trapped, mercury diffusion, bakeable vacuum system capable of obtaining a pressure of 2×10^{-10} torr. The normal background pressure for the experiments described below was about 5×10^{-9} torr. Extremely pure He was admitted to the system through a heated Vycor tubing; a He pressure of about 4×10^{-3} torr was used to obtain field ion patterns of the W tip. Xe was obtained from a flask of spectroscopically pure Xe gas (less than 100 ppm impurities) and admitted into the experimental tube through a liquid N_2 cooled, Ti gettered trap to remove active gases. The Xe pressure in the tube during ion gun operation was 6×10^{-5} torr, well below the pressure at which charge exchange effects became noticeable (about 3×10^{-4} torr for this tube geometry). The experimental tube was separated from the diffusion pump of the system by a ground glass valve, which permitted raising the He or Xe pressure in the tube to the necessary levels, and yet allowed rapid removal of the gas when desired.

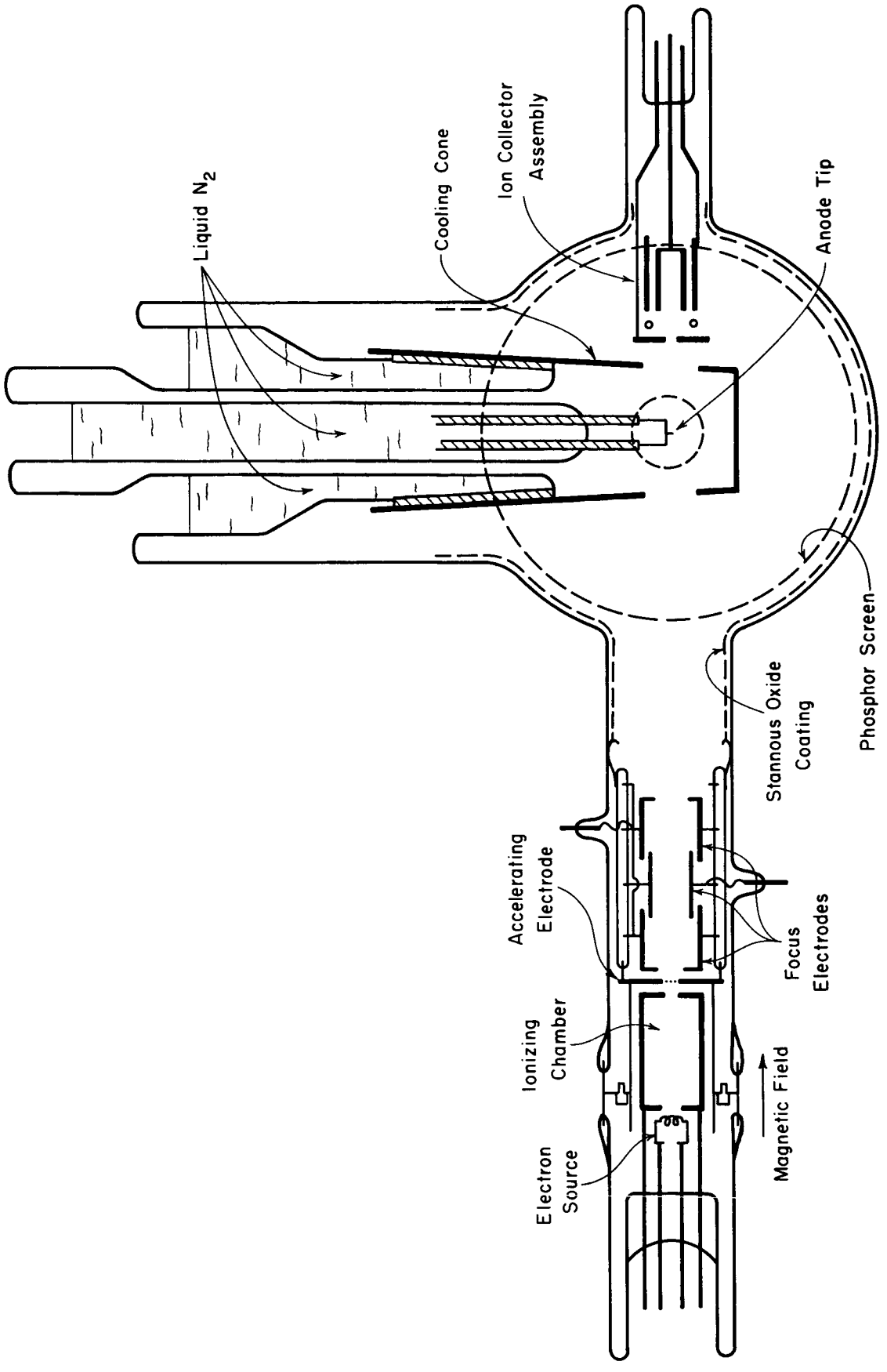

Figure 13. Schematic diagram of field ion microscope used for xenon ion sputtering of tungsten.

The experimental procedure for this study was the following: (1) The tube was filled with He, the tip surface was cleaned by field evaporation at a field of approximately 500 Mv/cm, and a photograph was taken of the resulting field ion pattern of the clean W surface at a viewing field of about 450 Mv/cm (Figure 14 (a)). (2) The He was pumped out and Xe was admitted with the viewing field still being applied to the tip; this prevented any contaminating atoms from reaching the tip during this step. (3) When the ion gun was ready to operate, the field was reduced to zero and the tip was bombarded with Xe ions. During this step the region around the tip was field-free; thus the bombarding ions hit the tip on only one side and the ion current density could be determined accurately. Also this was the only step during which impurity atoms could reach the anode surface. (4) After raising the field to 450 Mv/cm, the Xe was pumped out and He admitted in order to photograph the field ion pattern of the sputtered surface.

Results

Figure 14 (a) is a typical field ion pattern of clean W; Figure 14 (b) identifies the major crystal planes and a few of the minor ones. The many rows of small net planes extending inward toward the central (110) plane indicate that the anode tip was formed of a highly pure and nearly perfect single crystal of W. There are a few edge vacancies and crystal imperfections visible in the pattern; this amount of disorder is very small compared to that created by the sputtering of a few hundred ions. The bright spots around the edge of the pattern result from the method of cleaning used, and are not significant.

Figure 15 (a) shows the surface in Figure 14 (a) after being sputtered by 1200 ions of 500 ev energy (the ion beam is incident on the left side of the tip). By direct comparison of Figure 15 (a) with Figure 14 (a), a wealth of sputtering detail may be discovered; for example, the (433) plane near the lower edge of the pattern contains 10 atoms in its top atom layer in Figure 14 (a), but in Figure 15 (a) only 5 atoms remain. Just below the (433) plane a two-atom chain is missing, and the small net plane to the lower left of the (433) has two new vacancies. (The location of new, displaced and missing atoms in two successive ion patterns is greatly facilitated by Müller's color comparison technique[21], which was used extensively in the present analysis.) In general it can be seen that very little sputtering occurs on the uppermost atom layers of the major planes (the $\{110\}$'s, the $\{100\}$'s and the $\{211\}$'s) and that most of the sputtering damage is visible in regions lying between two major planes. Surprisingly, slightly more atoms are missing or displaced on the side away from the ion beam than on the side upon which it is incident.

Not all of the changes between Figures 14 (a) and 15 (a) are due to sputtering; a few are the results of impurity atoms. Figure 15 (b) was taken under the same conditions that Figure 15 (a) was taken except that no

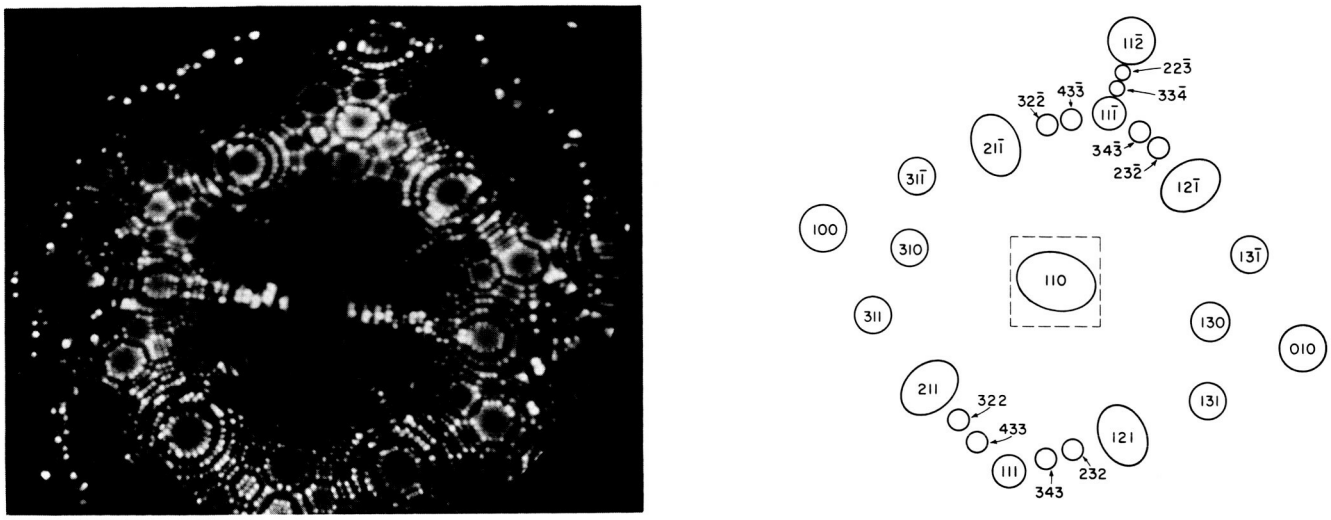

(a) (b)

Figure 14. (a) Typical field ion pattern of a clean and nearly perfect tungsten surface.
(b) Principal planes of a (110)-oriented bcc crystal corresponding to (a).

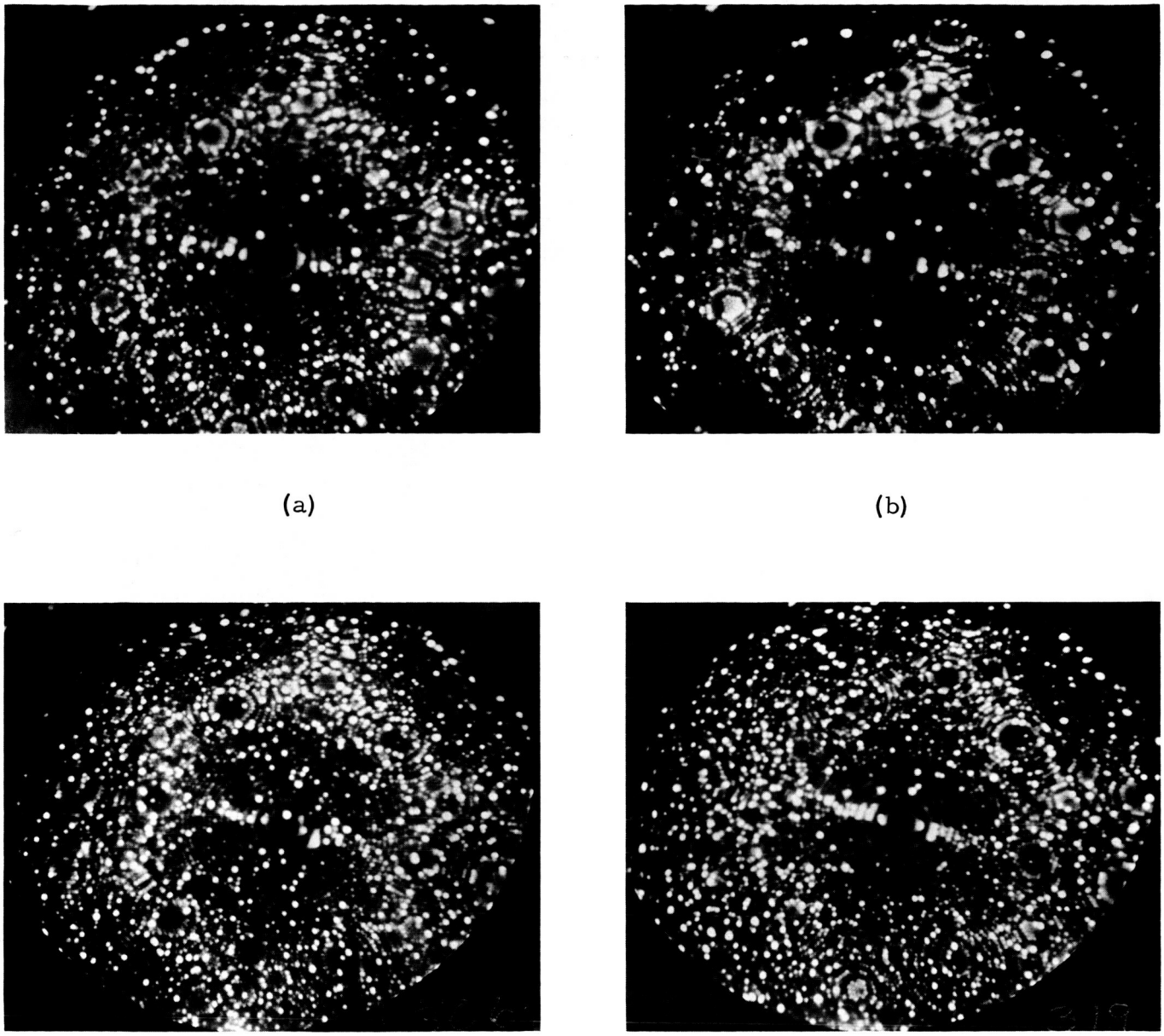

Figure 15. Field ion patterns of xenon ion sputtering of clean tungsten: (a) $N \approx 1200$ ions, $E_p = 500$ v; (b) Impurity pattern corresponding to (c); (c) $N \approx 200$ ions, $E_p = 100$ v; (d) $N \approx 1500$ ions, $E_p = 1300$ v. Ion beam is incident upon left side.

ions were allowed to hit the tip; thus the changes in Figure 15 (b) are due to impurity atoms only. The color comparison technique reveals that impurities not only add a few atoms to the surface which remain at the best viewing field, but also remove some tungsten atoms, primarily from the edges of net planes, as the field is raised up to the best viewing field[22]. These effects were in general a small fraction of those due to sputtering, and were randomly distributed over the pattern.

Figure 15 (c) was taken after bombardment of the anode tip by 200 ions with 100 ev energy. Although not too clear in Figure 15 (c) (but made clear by the color comparison technique) most of the changed atoms on the beam-incident side are added atoms, while most of the displaced and missing atoms are on the opposite side. For the 1300-ev ions (Figure 15 (d)) far more damage is done on the beam-incident side than on the opposite side, and there is very little dependence of damage upon crystallographic direction. These results may be explained qualitatively on the basis of a computer study by Gibson, et al.[23], of radiation damage in Cu. This study shows, among other things, that (1) energy can be transmitted long distances along close-packed atom chains (as first suggested by Silsbee[24]), and (2) above a certain energy (30 ev for Cu) the atom chains begin to defocus the transmitted energy and become increasingly inefficient at transmitting energy as the input energy is raised. Since in a bcc crystal like W there are two $[1\bar{1}1]$ atoms chains lying in the (110) plane, every point on the opposite side of a $\langle 110 \rangle$-oriented tip (which can be regarded as a stacking of 110 planes parallel to the ion beam axis) is connected to the beam-incident side by a close-packed atom chain. Thus at low energy (100 ev) a large fraction of the energy is transmitted through the crystal and causes atom ejection or displacement on the opposite side, whereas at high energy (1300 ev) energy transmission becomes inefficient and sputtering occurs primarily on the beam-incident side.

The number of displaced and missing atoms in different regions of the sputtered patterns were determined by counting all such atoms in an area whose size is indicated by the dashed square in Figure 14 (b) and which was centered on a particular plane. (Missing and displaced atoms in the same region of the corresponding impurity pattern were subtracted.) The results are given in Table IV and in general confirm the conclusion reached above. In addition the atom counts provide a rough estimate of the sputtering yield for each ion energy; these are also given in Table IV. When these yields are compared with yields obtained by another method[25], it can be seen that the 1300 ev yield is reasonable, the 500 ev yield is too low for reasons unknown, and the 100 ev yield is too high by an order of magnitude. The high yield obtained for 100 ev ions is attributed to the small size of the target: the distance between the (211) and (121) planes is approximately 300 atom diameters, a distance over which energy can readily be transmitted through the target and produce observable displacements on the far side, whereas the thickness of targets normally used for sputtering is sufficiently large that no energy is transmitted through to the back side.

TABLE IV

Atom Count Summary

Region	Bombardment Angle	Displaced and Missing Atoms at 100 ev	500 ev	1300 ev
110	90°	0	0	0
111	90	5	4	3
100	45	8	0	R[a]
310	63	9	16	R
31$\bar{1}$	65	10	20	R
211	73	0	6	38
322-433	82	3	12	35
010	135[b]	5	1	1
130	117	13	8	11
131	115	21	19	3
12$\bar{1}$	107	14	12	18
23$\bar{2}$-34$\bar{3}$	98	15	24	15
Sputtering Yield (atom/ion)		0.7	0.25	>1

Notes:
[a] R - damage too great to permit atom counting in this region
[b] Angles greater than 90° indicate the region is on the side opposite to which ion beam is incident

The depth of sputtering damage has been examined by removing through field evaporation successive atom layers from the surface of the target; Figure 16 is a series of ion patterns taken while field evaporating atom layers from the tip sputtered by 1300-ev ions (Figure 15 (d)). It shows that the damage is primarily on the beam-incident side, and persists to a depth of approximately 6 (110) atom layers. In contrast, almost all of the damage due to 100-ev ions is removed by the field evaporation of one atom layer. An interesting feature of Figures 16 (b) and 16 (c) are the bright spots appearing at random over the central portions of the ion patterns; these bright spots are attributed to impurity atoms lying just below the surface[20]. In this case the impurity atoms are very likely to be Xe atoms; Kornelsen, et al.,[26], have shown that 1% of 1300-ev Xe ions can penetrate a depth greater than 8 atom diameters in W.

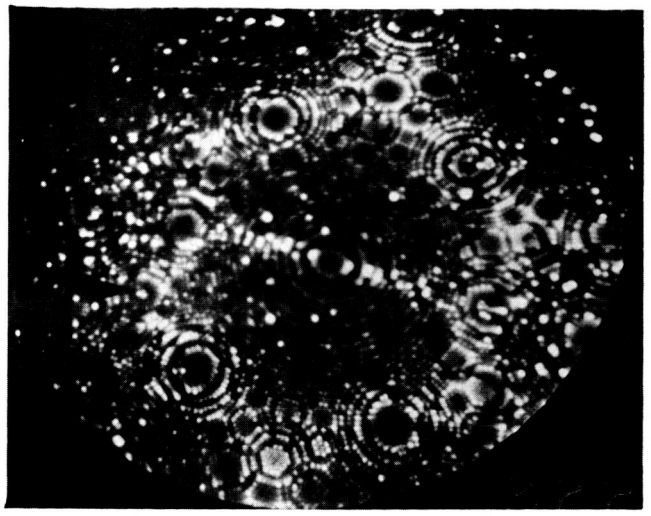

(a)

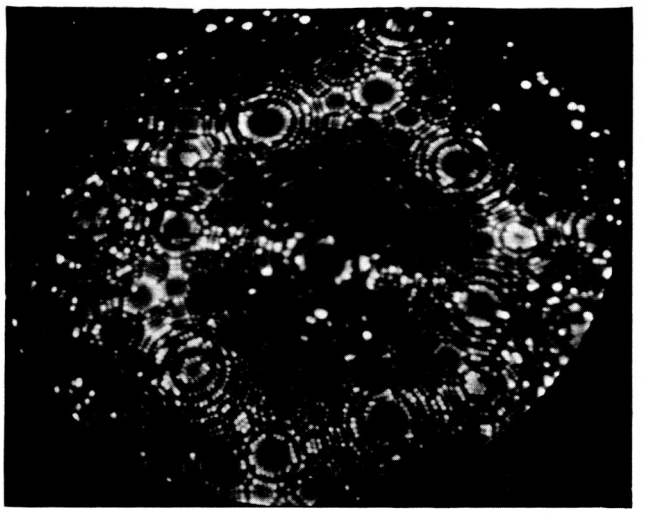

(b)

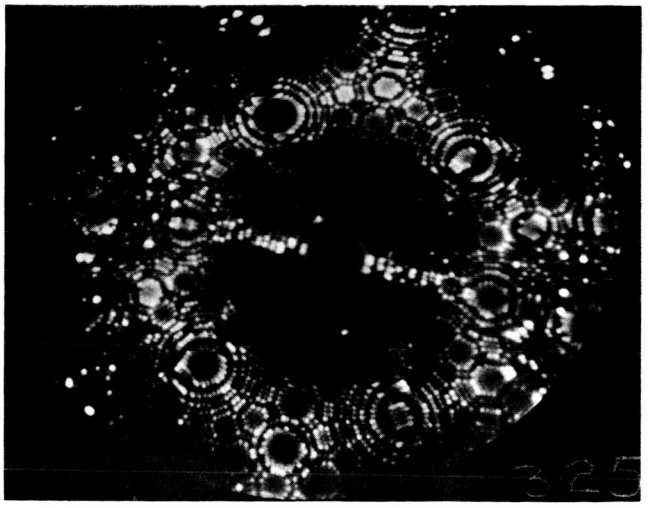

(c)

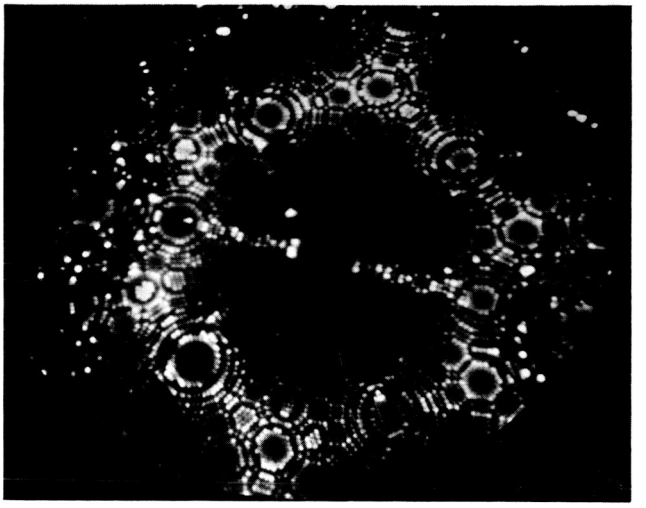

(d)

Figure 16. Field ion patterns illustrating the depth of damage due to 1300 v sputtering as revealed by the total number of (110) layers removed by field desorption: (a) one, (b) two, (c) four, (d) six.

REFERENCES

1. L. W. Swanson, et al., NASA CR-54106 (Field Emission Corporation, 1964).

2. Quarterly Report No. 2 for NASA Contract NAS3-5902 (Field Emission Corporation, 1 September 1964 to 30 November 1964).

3. Quarterly Report No. 1 for NASA Contract NAS3-5902 (Field Emission Corporation, 3 June 1964 to 31 August 1964).

4. C. J. Bennette, et al., J. Appl. Phys. 35, 3054 (1964).

5. Report No. 2 for NASA Contract NAS3-2596 (Field Emission Corporation, 1 December 1963 to 29 February 1964).

6. J. P. Barbour, et al., Phys. Rev. 92, 45 (1953).

7. Linfield Research Institute, Quarterly Report No. 6, Contract No. NObsr 72697, Index No. NE-110000, 1 August 1958 to 31 October 1958.

8. G. E. Vibrans, Technical Report 353, Lincoln Laboratory, M.I.T. (8 May 1964).

9. G. E. Vibrans, Technical Report 308, Lincoln Laboratory, M.I.T. (18 April 1963).

10. W. P. Dyke, et al., Phys. Rev. 91, 1043 (1953).

11. W. W. Dolan, et al., Phys. Rev. 91, 1054 (1953).

12. E. E. Martin, et al., J. Appl. Phys. 31, 782 (1960).

13. L. W. Swanson, et al., Final Report for NASA Contract NASw-458 (Field Emission Corporation, 1963).

14. AIP Handbook, ed. by D. W. Gray (McGraw-Hill Book Co., Inc., New York, 1963) pp 9-149.

15. Quarterly Report No. 3, Contract PH 43-64-71 (NIH), (Field Emission Corporation, 26 January 1965) p 7.

16. L. W. Swanson, et al., NASA CR-22 (1964).

17. D. Menzel and R. Gomer, J. Chem. Phys. 41, 3311 (1964).

18. D. Menzel and R. Gomer, J. Chem. Phys. 41, 3329 (1964).

REFERENCES (continued)

19. R. Gomer and L. Swanson, J. Chem. Phys. 38, 1613 (1963).

20. E. W. Müller, in Direct Observations of Imperfections in Crystals, ed. by J. B. Newkirk and J. W. Wernich (Interscience Publishers, New York, 1962) 77.

21. E. W. Müller, J. Appl. Phys. 28, 1 (1957).

22. J. F. Mulson and E. W. Müller, J. Chem. Phys. 38, 2615 (1963).

23. J. B. Gibson, et al., Phys. Rev. 120, 1229 (1960).

24. R. H. Silsbee, J. Appl. Phys. 28, 1246 (1957).

25. D. Rosenberg and G. K. Wehner, J. Appl. Phys. 33, 1842 (1962).

26. E. V. Kornelsen, et al., Phys. Rev. 136, A849 (1964).